Biosensors and Bioelectronics 122 (2018) 189–204

Contents lists available at ScienceDirect

Biosensors and Bioelectronics

journal homepage: www.elsevier.com/locate/bios

Patchable micro/nanodevices interacting with skin

Wubin Bai[b,1], Tairong Kuang[a,*,1], Chandani Chitrakar[c], Ruiguo Yang[d], Shulin Li[e], Donghui Zhu[c], Lingqian Chang[c,*]

[a] Key Laboratory of Polymer Processing Engineering of Ministry of Education, South China University of Technology, Guangzhou, PR China
[b] Department of Materials Science and Engineering, Center for Bio-Integrated Electronics, Northwestern University, Evanston, IL, USA
[c] Department of Biomedical Engineering, University of North Texas, Denton, TX, USA
[d] Department of Mechanical and Materials Engineering, University of Nebraska-Lincoln, Lincoln, NE, USA
[e] Department of Pediatrics, University of Texas MD Anderson Cancer Center, Houston, TX, USA

ARTICLE INFO

Keywords:
Skin-patchable devices
Micro/nanodevices
Gene/drug delivery
Wearable sensors
Single cell

ABSTRACT

Patchable devices that interface with the skin across a wide range of size scales, from cellular level down to molecular level, become increasingly attractive in biomedical research. These devices hold the potential for diagnostic and therapeutic functions with exceptional spatiotemporal precision, continuity, and convenience. Further, they afford new opportunities to integrate cloud-based technology and artificial intelligence for a smarter healthcare system. This article reviews recent advances in materials design and assembly techniques for fabricating various patchable devices, with focuses on electrical, thermal, mechanical, and chemical biosensors as well as transdermal gene and drug delivery platforms. A concluding discussion provides perspectives for future developments and outlooks in clinical applications.

1. Introduction

Medical diagnosis is the essential basis for targeted treatments; while many failed medical treatments arise from ambiguous or delayed diagnostic results (Liu et al., 2017). Skin provides the outmost pathway for diagnosis and therapeutic options throughout the whole body (Son et al., 2014). A number of epidermal diagnostic methods have been developed, ranging from reading electrophysiological signals, including electrocardiography (ECG), electroencephalography (EEG), electromyography (EMG) (Jang et al., 2016; Xu et al., 2014; Yeo et al., 2013; Zhu et al., 2018), recording tissue temperatures (Gao et al., 2014; Trung et al., 2016; Webb et al., 2013; Wu et al., 2015a; Yang et al., 2015) and characterizing its thermal and mechanical properties, such as blood pressure (Dagdeviren et al., 2015b; Lee et al., 2016b; Li et al., 2016; Liu et al., 2016; Luo et al., 2016; Tian et al., 2017; Webb et al., 2015; Zhang et al., 2015) to measuring the biochemical balance of the body fluids (Chen et al., 2017; Gao et al., 2016b; Koh et al., 2016; Martin et al., 2017). Epidermal therapeutic capabilities typically include skin phototherapy (Jain et al., 2016; Kearney et al., 2014), thermal/electrical stimulation (Hong et al., 2015), local drug delivery (extracellular) and direct cell transfection (intracellular) (Dul et al., 2017; Pires et al., 2018). A wide variety of materials with engineered architectures at the micro and nano scale introduce additional advantages in miniaturized physical dimensions as well as low weight and power consumption, which leads to improved mechanical flexibility, and enhanced operational sensitivity or functionality for skin-patchable devices (Kim et al., 2011; Rogers et al., 2011; Trung and Lee, 2016).

Recent advancements in skin-patchable devices include: i) a clear transition initiating from single functional device to multifunctional comprehensive analysis platform via on-chip integration (Chang et al., 2016a; Gao et al., 2017; Imani et al., 2016; Yang et al., 2015); ii) novel devices gaining capabilities in delivering stimulation triggers (such as electrical pulses, optical pulses, and thermal fields) through the skin to interact with subcutaneous tissues, including free nerve endings, and muscles, narrowing down to a targeted single cell (Xu et al., 2016). Interestingly, the new emergence of a patching nano-transfection chip that can directly transfect genes with high molecular-weight plasmids into skin cells, leading to successful reprogramming of the epidermis and dermis into other functional somatic cells, e.g. induced neurons (iNs), shows a paradigm shift from previous methods (Gallego-Perez et al., 2016). All these pioneering prototype devices offer efficient and continuous *in vivo* treatments without causing inconvenience to the user's natural activities (Paulussen et al., 2015; Wang et al., 2017a; Wang et al., 2017b). With a prospect in clinical applications, some of

* Corresponding authors.
E-mail addresses: kuangtr@scut.edu.cn (T. Kuang), Lingqian.chang@unt.edu (L. Chang).
[1] These authors contributed equally to this workwork.

https://doi.org/10.1016/j.bios.2018.09.035
Received 26 June 2018; Received in revised form 9 September 2018; Accepted 10 September 2018
Available online 11 September 2018
0956-5663/

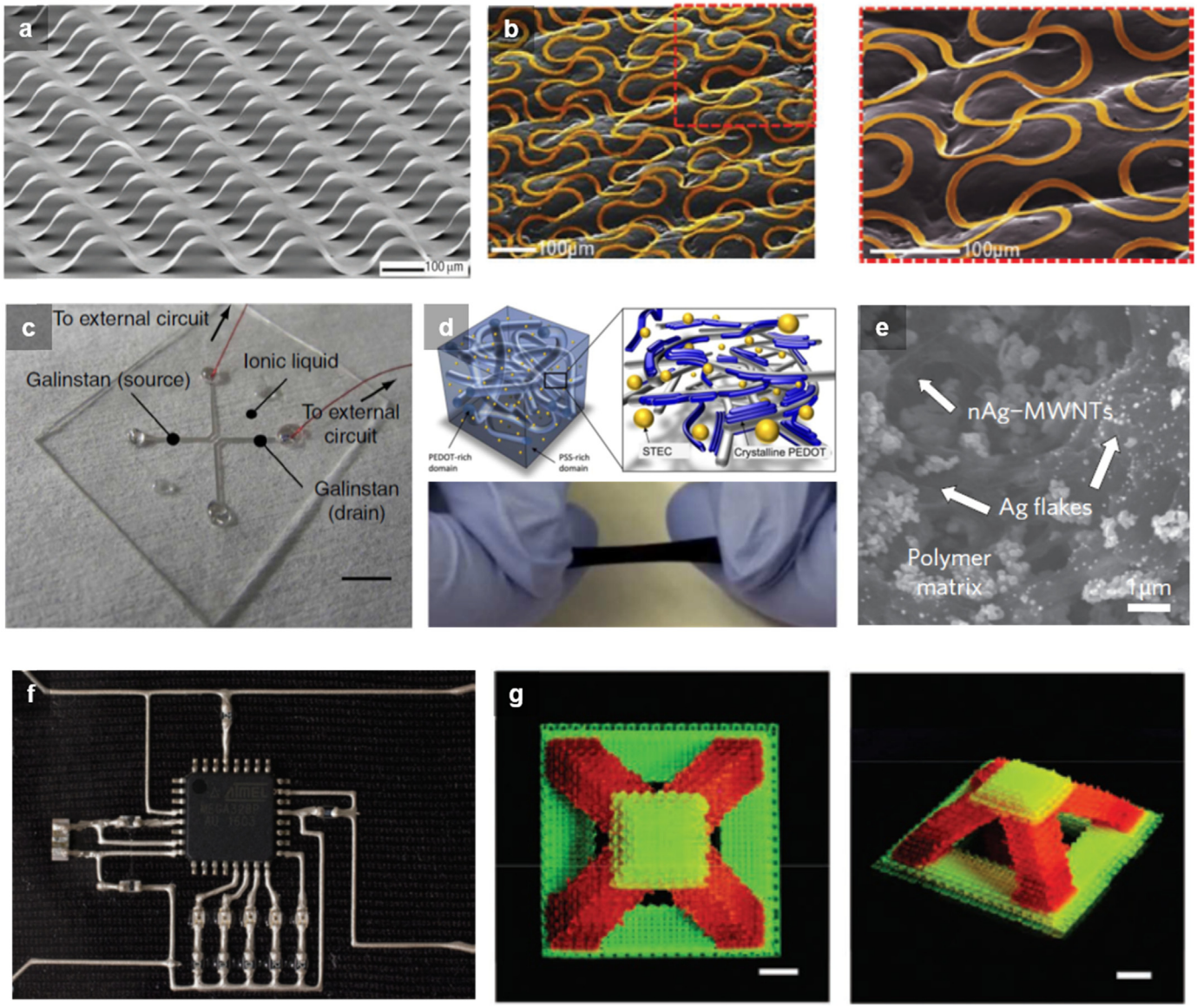

Fig. 1. Key materials and techniques for forming patchable devices. (a) Controlled buckling of semiconductor nanoribbons for stretchable electronics. In this case, Si ribbon structures are formed on a PDMS substrate pre-strained to 50% and patterned with parallel lines of adhesion sites (Wact = 15 μm and Win = 250 μm) oriented at angles of 30° with respect to the lengths of the ribbons. The image was taken by tilting the sample at an angle of 75°. Reprinted with permission from Nature (Sun et al., 2006) (b) A multifunctional epidermal electronic system, in ultrathin formats, robustly bonded to and encapsulated on the skin. Reprinted with permission from Wiley.(Yeo et al., 2013) (c) Fully fabricated liquid heterojunction device consisting of an ionic liquid active channel and GaInSn source/drain electrodes (scale bar, 2.5 mm). Reprinted with permission from Nature.(Ota et al., 2014) (d) A highly stretchable, transparent, and conductive polymer made of poly (3,4-ethylenedioxythiophene): poly(styrene sulfonate) and enhancers of ionic additives-assisted stretchability and electrical conductivity. Reprinted with permission from AAAS (Wang et al., 2017e). (e) High conductive, printable and stretchable composite films of carbon nanotubes and silver. A SEM image of an Ag-multiwalled carbon nanotube composite films. Reprinted with permission from Nat Nanotechnol (Chun et al., 2010). (f) Image of microcontroller circuit fabricated by hybrid 3D printing, in which surface mount electrical components are interconnected with printed AgTPU electrodes onto an underlying TPU matrix. Reprinted with permission from Wiley (Valentine et al., 2017). (g) 3D printing of large-scale, high-resolution living responsive materials and devices. The living responsive materials include hydrogel ink, chemicals, and bacterial cells. Reprinted with permission from Wiley (Liu et al., 2018).

these biomedical devices show promise on comprehensive functionality, considering not only disturbance-free and meticulous examination but also timely treatment.

Emerging techniques such as soft lithography (molding, embossing, and transfer printing) (Shim et al., 2014; Xia and Whitesides, 1998), 3D printing (Gladman et al., 2016; Lewis and Ahn, 2015), laser cutting (Bartlett et al., 2016; Yang et al., 2015), and roll-to-roll printing enable heterogeneous integration of a wide spectrum of materials (Deng et al., 2015; Yeo et al., 2014) in fabricating skin-patchable micro-/nano-scale devices. Soft lithography inherits capabilities from conventional wafer-based microfabrication methods and enables wider choices of materials and their hybridizations. Laser cutting and 3D printing provide efficient and prototyping-oriented solutions for designing complex and functional 2D and 3D patterns (Axisa et al., 2012; Yang et al., 2015). Roll-to-roll printing and step-and-flash imprinting scale up manufacturing production and lower the fabrication cost (Deng et al., 2015; Yeo et al., 2014).

In this review, we highlight recent advances in patchable micro-/nano-devices interacting with the skin. We first summarize representative designs of materials and fabrication strategies currently reported in fabricating skin patchable devices. Different from existing excellent reviews (Lee et al., 2017; Liu et al., 2017; Patel et al., 2012;

Prausnitz and Langer, 2008; Prausnitz et al., 2004; Stoppa and Chiolerio, 2014; Windmiller and Wang, 2013; Zhang et al., 2017a; Zhao and Huang, 2017), we focus more on the novel functions of these biomedical devices and their capabilities toward single cell *in vivo* application. In terms of materials, most of these devices are fabricated on a flexible substrate made from nanomaterials or polymers; some recent reports demonstrated skin patches on rigid silicon. Subsequently, we discuss electric sensing devices for physiological signal detection based on direct electrical contact or capacitive-coupled sensors, and then introduce representative thermal sensing devices that enable clinical opportunities in wound healing. In the following section after this, we focus on mechanical sensors coupled with electrical systems to serve as mechanoreceptors in various applications, ranging from neural-integrated touch monitoring to epidermal viscoelasticity sensors. We also discuss patchable devices for chemical sensing on metabolically-essential ionic or organic molecules, of which the concentration can be utilized to determine the pathological condition of the body. One of our highlights is the next generation transdermal gene delivery patching platform. Beyond chemical particles and needles, novel technologies show possibilities of direct gene transfection of skin cells facilitated by advanced nanoneedles, sonoporation, laser and nano-electroporation, thus overcoming the challenges in transporting macromolecular drugs, naked DNAs, and genes into the epidermis or dermis. Preclinical potentials have been also witnessed in specific fields *in vivo*, including wound healing, pathological studies, gene editing, and regenerative medicine. In the last section, we discuss some typical issues remaining for the current devices, and give prospects for future development toward a multimodal system with high reliability for clinical applications in medical diagnosis and therapy.

2. Key materials and fabrication techniques in fabricating patchable devices

One essential consideration for wearable devices is the way to achieve intimate contact with the skin with minimum invasiveness (Khan et al., 2016; Liu et al., 2017; Lu and Kim, 2014; Zhao and Huang, 2017; Chu et al., 2016; Heikenfeld et al., 2018). This requires a special design of the constituent materials, especially for those lack of mechanical flexibility in their bulk geometries, such as semiconducting materials and metals (Rogers et al., 2011). Typically, human skins can deform up to 15% of strain level with an elastic moduli ranging from 10 kPa to a few hundred kPa (Liang and Boppart, 2010). Patchable devices tend to have sufficient bendability and stretchability to attach to the skin conformally and accommodate mechanical bending/stretching caused by external forces or body motion. A straightforward way to modify the flexibility of a specific material is to prepare them in ultrathin layers, since the flexural rigidity or mechanical resistance of a material is proportional to the thickness of the material to the third power (Jeong et al., 2013; Rogers et al., 2010). For example, the transfer printing technique deliver high-quality monocrystalline silicon nanomembranes from a silicon-on-insulator substrates onto pre-stretched elastic polymer substrates with selective bonding sites. Such hybrid integration with 3D-bulk serpentine-shaped silicon ribbons supported by an intrinsically soft substrate, offers novel electronic properties, high mechanical bendability and stretchability (Fig. 1**a**) (Sun et al., 2006). Such transfer-printing strategies can also be applied to conductive metal membranes, such as films of gold, copper, and platinum, with serpentine-like patterns defined by traditional photolithography to yield a certain degree of stretchability (Fig. 1**b**) (Yeo et al., 2013).

Other ways to achieve flexibility starts with introducing unconventional materials, such as functional polymers, hydrogels, and functional liquids, that can intrinsically preserve mechanical and other desired properties. Composites of multiple materials for realizing synergetic performances under multiple requirements represent another promising avenue for fabricating skin-patchable devices. Materials in the liquid state offer a high geometrical adaptability, thus are suitable for serving as active electronic components embedded inside a soft elastomeric matrix to build highly deformable devices with sensing capabilities (Fig. 1**c**) (Ota et al., 2014). Conductive polymers, a class of intrinsically stretchable molecular materials with advantages in patterning approaches, show promising improvements in electronic performance via engineering polymer components and additives (Fig. 1**d**) (Wang et al., 2017e). Mixing nano-scale conductive fillers with elastomeric polymers can form a nanocomposite that yields both mechanical flexibility and electrical conductivity, of which their dependences on temperature, humidity, and strain can enable fabrication of associated sensors (Fig. 1**e**) (Miyamoto et al., 2017).

Soft lithography exploits elastomeric elements not only as stamps for delivering nontraditional materials with nanometer dimensions or larger onto planar or nonplanar surfaces at low cost, but also as soft molds for imprinting targeted materials into designated patterns and for forming complicated 3D structures (Rogers and Nuzzo, 2005). Besides soft lithography, additive printing (e.g. 3D printing, inkjet printing) provides another route toward fabricating patchable devices with high programmability, scalability, and low barrier-to-entry (Fig. 1**f**) (Valentine et al., 2017). This approach further enriches the platform with wider choices of materials, including biomolecules, cells, liquid metals, biomimetic materials and ceramics (Fig. 1**g**) (Liu et al., 2018). Some types of materials or hybrid combinations of them, such as in silicon-nanomembrane photodetectors (Lu et al., 2018), and electrodes made of organophosphorus hydrolase (Mishra et al., 2018), enable fabrication of active devices that generate signals (in the form of electrons, photons or others) in response to the interaction with the targeted skin area, while other devices deliver sensing information via modulating or harvesting existing signals generated from an external source (Kang et al., 2016). In particular, wireless technologies, that are coupled with patchable devices for data collection, includes near-field communication, bluetooth, and optical colorimetry (Gao et al., 2014; Nag and Mukhopadhyay, 2015; Xu et al., 2015).

3. Patchable devices for electrical sensing

Patchable devices that sense the electrical signal (in the form of voltages for ECG, EEG, and EMG, ranging from μV to mV) from the skin require two or more metal electrodes, and effective electrical contact via conformal laminating probes onto the targeted skin area (Yang et al., 2017). The electric sensors discussed in this section can be classified by the type of electrical contact: direct contact or capacitive contact (Jeong et al., 2012; Jeong et al., 2014; Kim et al., 2011; Lee et al., 2014; Mostafalu and Sonkusale, 2015; Myers et al., 2015; Yang et al., 2015; Yu et al., 2013). As typical electrical sensors do not interfere with operations of mechanical, thermal or optical sensors, it is also possible to form multi-function sensor arrays (Imani et al., 2016; Kim et al., 2011; Liu et al., 2016; Yamada et al., 2011; Yang et al., 2015).

3.1. Design of electrophysiological (EP) sensors

Measurements of EP data enable assessments of physical and mental state, sleep disorder, cardiac diseases, brain tumor, ischemia and stroke (Banaee et al., 2013; Bonato, 2003, 2010; Patel et al., 2012). The direct electrical contact of the EP measurements is made by conformally laminating a biocompatible conductive layer, such as gold films, gallium liquid, carbon nanotubes and platinum nanowires on the skin (Jeong et al., 2012; Kim et al., 2011; Lee et al., 2014; Mostafalu and Sonkusale, 2015; Yang et al., 2015; Yu et al., 2013). The voltage between two of such electrodes is amplified by either an on-chip Si nanomembrane-based transistor for lower noise level (Fig. 2**a**), or by an external amplifier for lower cost (Fig. 2**b**). The filamentary serpentine pattern of the Si nanomembranes and Au electrodes enhances the mechanical strength of the device. Both designs enable a promising signal-to-noise ratio for a

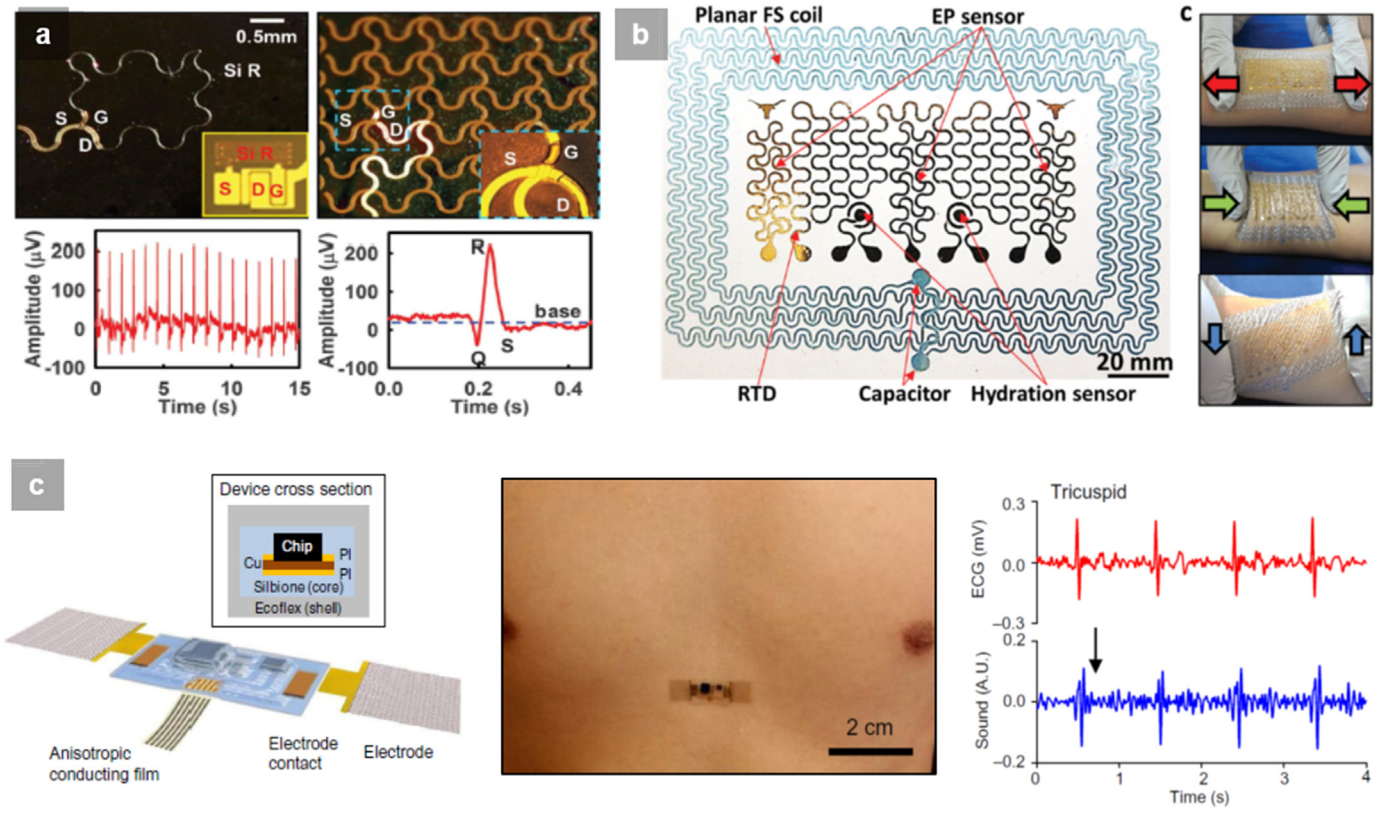

Fig. 2. Patchable electrical biosensors using various fabrication techniques and sensing mechanisms (a) Optical micrographs of an active electrophysiological (EP) sensor with on-chip amplification, as part of an FS-EES. (Left) The source, drain, and gate of a silicon MOSFET and a silicon feedback resistor before connection to sensor electrodes, all in FS layouts. (Inset) Similar device with island design. (Right) The final device, after metallization for the interconnects and sensor electrodes, with magnified view (inset). Bottom: ECG signals measured with an active EES attached to the chest (left), and magnified view of data corresponding to a single heartbeat (right). Reprinted with permission from AAAS (Kim et al., 2011). (b) Illustration of the assembled device and its interface with soft EP measurement electrodes and flexible cable for power supply and data acquisition. A cross-sectional view appears in the upper inset. Middle image of an epidermal device mounted on the chest. Comparison of heart sound signals measured using a commercial electronic stethoscope and the reported device. Reprinted with permission from AAAS (Liu et al., 2016). (c) Multi-material, multiparametric ESS. Left: Top view of an ESS which incorporates three EP electrodes (Au-PET), a resistance temperature detector (RTD) (Au-PET), two coaxial dot-ring impedance sensors (Au-PET), and a wireless planar stretchable strain sensing coil (Al-PET), all in filamentary serpentine (FS) layout. ESS on human skin demonstrating excellent deformability during stretch (top), compression (middle), and shear (bottom). Reprinted with permission from Wiley (Yang et al., 2015).

high-resolution ECG signal detection in as low as hundreds of microvolts, as evidenced by the observed clear Q, R and S peaks (Fig. 2**a**).

Separating the electrodes and the skin with a thin layer of dielectric material yields capacitively-coupled contacts (Fig. 2**c**). A gold polyimide (PI) bilayer or silver nanowires embedded in a polydimethylsiloxane (PDMS) layer is used to realize this configuration (Jeong et al., 2014; Myers et al., 2015). It provides a complete encapsulation of the electrodes, avoiding electrical leakage and shorting, and enabling the reusability of the sensors, as they can be easily detached from the skin without damaging the circuit. The properly designed capacitance also acts as a high-pass filter, allowing the measurement of ECG signals while filtering out the low-frequency component from the environment. The sensitivity of capacitive-coupled electrodes is comparable to the electrodes in direct contact mode (Fig. 2**c**).

3.2. Integration with other sensors

A typical integrated sensor array consists of an EP sensor, reference and ground electrodes, a filamentary serpentine resistive thermometer, a capacitive hydration sensor and an LC oscillation-based wireless strain sensor (Fig. 2**b**) (Yang et al., 2015). Other available components that have been reported so far include flexible solar cells and radio-frequency (RF) coils for powering (Kim et al., 2011), light-emitting diodes (LEDs), photodetectors for optical sensing (Imani et al., 2016; Kim et al., 2011; Yamamoto et al., 2017), and acoustic sensors as an auxiliary measurement for high-validity ECG signals (Fig. 2**c**) (Imani et al., 2016; Liu et al., 2016).

4. Patchable devices for thermal sensing

Patchable thermal sensors or epidermal thermometry enables measurements of thermal properties of skin, creating clinical opportunities in wound treatment or healing monitoring, cancer screening, sleep monitoring (Han et al., 2018), core body temperature assessments (Gao et al., 2014), and cardiovascular health evaluation (Webb et al., 2013). The capability of epidermal thermometry in continuous, non-invasive, cost-effective, and mK-precision mapping of epidermal temperature is realized not only at lower cost, as compared to a typical infrared digital camera, but also in a manner compatible with natural motions or behaviors of users.

The ideal epidermal temperature sensors rely on effective isolation from applied strains both internally and externally, minimal perturbations, and conformal attachment (Gao et al., 2014; Webb et al., 2013), which can be achieved via integration of open-mesh, interconnected serpentine layouts (mostly for tensile strain relief), a neutral mechanical plane construction (for wrinkle strain relief), and an ultrathin geometrical design (Webb et al., 2013). The sensor arrays can conform to the curved, textured surface of the skin as low interfacial stresses enable adequate adhesion through Van der Waals force (Gao et al.,

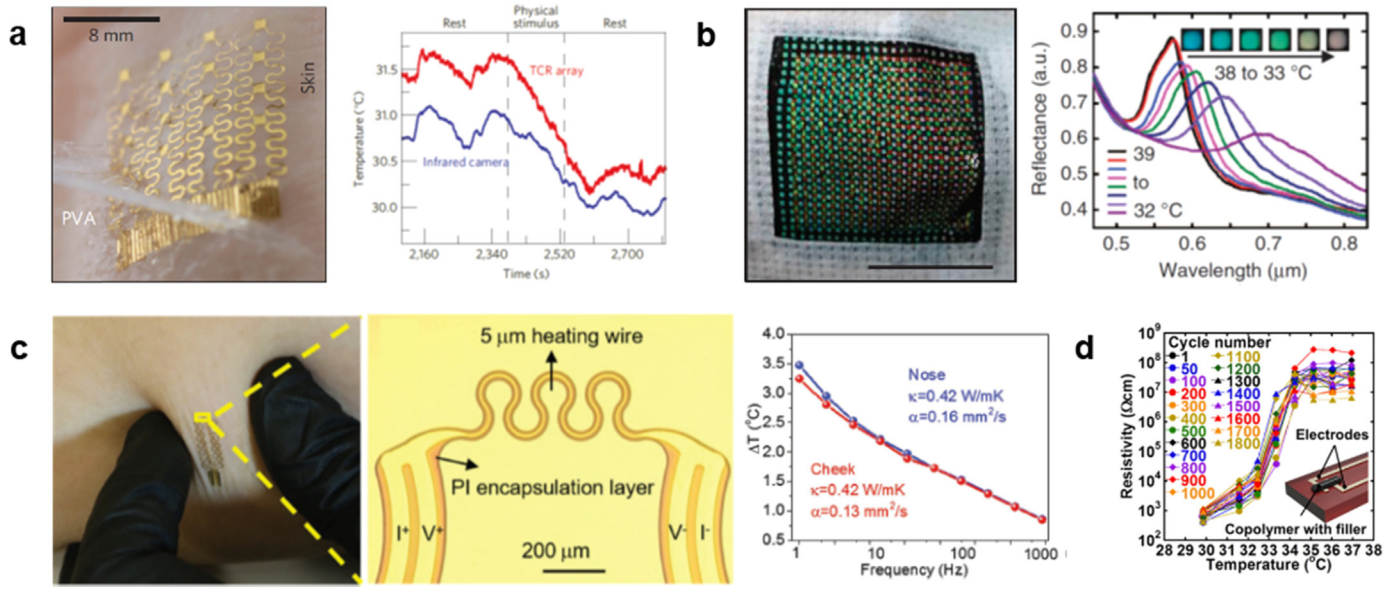

Fig. 3. Patchable thermal biosensors based on unconventional materials, sensing mechanisms, and diagnostic designs. (a) Ultrathin, compliant, skin-like arrays of precision temperature sensors and heaters, Image of a 44 TCR sensor array after application to the skin using a water-soluble adhesive tape based on poly (vinyl alcohol). The temperature of the palm measured with an infrared camera (blue) and a sensor array (red, offset for clarity) during physical stimulus tests. Reprinted with permission from Nature (Webb et al., 2013). (b) e-TLC thermal imaging device as an example of an epidermal photonic system. Picture of a device with calibration colors operating on the curved surface of the skin. Scale bar, 2 cm. Reflectance measured at a single pixel from 32 °C to 39 °C and corresponding images for 33 °C to 38 °C (inset). (Calibration and use of e-TLC devices for skin thermal imaging) Reprinted with permission from Nature (Gao et al., 2014). (c) Flexible and stretchable 3ω sensors. Photograph of a serpentine 3ω sensor printed onto a thin silicone substrate and applied to the skin of the forearm of a subject. Optical image of a serpentine wire composed of an Au heater (5 μm wide) and PI encapsulation layers (20 μm wide). Measured temperature oscillations from the 3ω sensors as a function of frequency. Reprinted with permission from Wiley (Tian et al., 2017). (d) Characteristics of tunable temperature sensors with high sensitivity. Cyclic, mechanical, and environmental stability of physiological temperature sensors. based on composites of semicrystalline acrylate polymers and graphite. Reprinted with permission from the National Academy of Science (Yokota et al., 2015).

2014; Webb et al., 2013). Patchable thermal sensors typically rely on either sensing probes made with thin, narrow serpentine traces of gold, or ultrathin, compliant, pliable sensor arrays those are driven by PIN diodes based on silicon nanomembranes. The latter devices are highly sensitive for subtle variations in skin temperature associated with mental activity, physical stimulation and vasoconstriction/dilation along with skin hydration (Fig. 3**a**) (Webb et al., 2013). Design dimensions for the metal-film based sensing probes are determined by the desired amplitude of temperature-sensitive electrical resistance, in which increasing resistance can enhance the sensitivity of temperature measurement. Hence, typical metal-based resistive thermal sensors tend to adopt a densely packed serpentine geometry to realize a sufficiently high resistance in a miniaturized space.

Thermochromic liquid crystals (e-TLC) are packaged via transferring large-scale, pixelated arrays of TLC materials onto thin elastomeric substrates. Conformal contact of TLC to the skin enables thermal sensing via the recording of their color change, which is resulted from the cholesteric phase of the microencapsulated chiral nematic liquid crystals exhibiting wavelength blueshift in light reflection upon increasing temperature (Fig. 3**b**). Precise measurements of thermal conductivity and thermal diffusivity is obtained through analysis of the resulting spatial-temporal images (Fig. 3**b**) (Gao et al., 2014).

Patchable devices that integrate the 3ω method into soft, flexible platform improves detection accuracy of the *in vivo* thermal transport on soft, curved tissues of living organisms, as the alternating current (AC) method is insensitive to DC noises or artifacts (Fig. 3**c**) (Tian et al., 2017). The controlled heating frequency also confines the thermal penetration depth of the testing area, which can be used for multi-layer measurements (Tian et al., 2017). In comparision, resistive thermal sensors and thermal couples typically measure temperatures that only reflect the surface of the contact area. A traditional thermal camera can reveal the temperature of a typical biological tissue at depths around 2 mm. It is, however, a challenge to calculate the corresponding thermal depth profile just from its surface recording (Pang et al., 2013; Stolik et al., 2000).

Ultra-flexible, printable thermal sensors (Fig. 3**d**) fabricated from composites of semicrystalline acrylate polymers and graphite particle fillers exhibit high temperature sensitivity (~ 20 mK), high cyclic stability (1800 times), and a fast response with a response time less than 100 ms under physiological conditions, which allows *in vivo* mapping of cyclic temperatures changes of 0.1 °C in the lung of a rat during breathing without interference from tissue motion (Yokota et al., 2015). In addition, incorporating thermal actuators to the thermal sensing platform extends the option of local skin heating for measurements of local thermal conductivity, hydration, blood-flow rate, and other important physiological information of relevance to dermatological and overall health (Webb et al., 2013; Tian et al., 2017; Yokota et al., 2015).

5. Patchable devices for mechanical sensing

Fig. 4**a** shows the design of a soft strain sensor based on liquid metals which exhibits a high tolerance of strain up to 200%. A conductive filling of galinstan liquid is embedded underneath a tactile diaphragm and confined inside PDMS microfluidic channels. This configuration enables electrical resistive modulations via channel geometrical deformation. The design is thus capable of detecting sub-50 Pa changes in environmental pressure with a response time of 90 ms (Fig. 4**a**), offering applicability in pulse sensing and tactile sensing (Gao et al., 2017). An ultraflexible strain sensor based on thin films of aligned single-walled carbon nanotubes utilizes the stretch-induced fracturing of nanotube films to form islands, gaps and bundles that bridge the gaps. The strain-dependent modulation of electrical resistance enables strain sensing (up to 280%) capability with high durability (10,000 cycles at 150% strain), fast response (14 ms) and low creep (3% at 100% strain) (Fig. 4**b**) (Yamada et al., 2011). Fig. 4**c** shows a conformal modulus sensors (CMS) made with ultrathin,

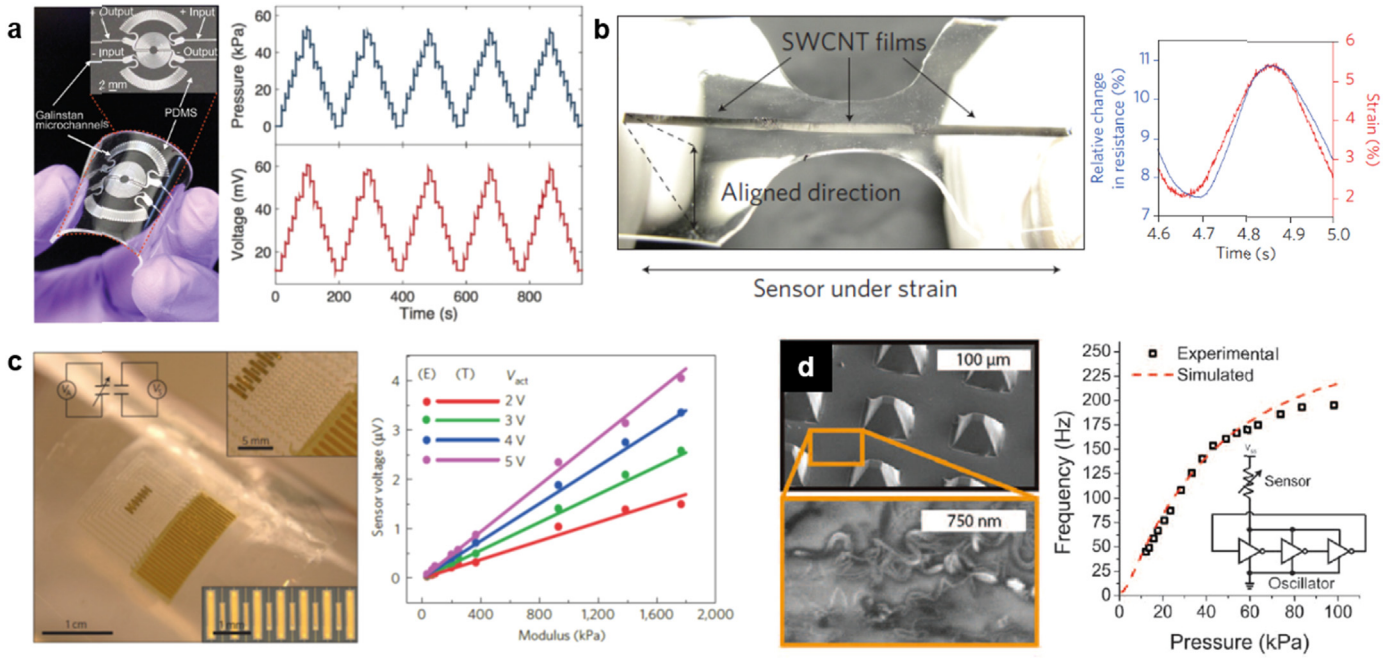

Fig. 4. Patchable mechanical biosensor for motion detection, epidermal diagnosis, and measuring essential physiological parameters. (a) Microfluidic tactile diaphragm pressure sensor. Left: Optical image of a finished microfluidic diaphragm sensor. Schematic layout of the diaphragm sensor. Assessment of the diaphragm pressure sensor. Inset: Optical image of the experimental setup used for testing. Right: Real-time monitoring of the output voltage change as the pressure is stepped up and down over five cycles. Reprinted with permission from Wiley (Gao et al., 2017). (b) Left: SWCNT-film strain sensor, aligned single-walled carbon nanotube (SWCNT). Right: Relative change in resistance (blue) during 2.5 Hz frequency cycling between 2.0% and 5.4% strain (red). Reprinted with permission from Nature (Yamada et al., 2011). (c) Left: Thin, compliant modulus sensor (CMS) based on nanoribbons of PZT in arrays of mechanical actuators and sensors. Photograph of a device on a thin silicone substrate. Optical microscope images of the interconnect region (upper-right inset), the actuator/sensor arrays (lower-right inset), and a simple electrical circuit diagram of actuators and sensors (upper-left inset). Right: Experimental and theoretical analysis of the device operation. Output voltage from sensor no. 1 as a function of the modulus of the substrate under test for four actuator voltages (Vact). Reprinted with permission from Nature (Dagdeviren et al., 2015a). (d) Oscillator and pressure sensor characteristics and integration. Scanning electron micrographs of the pyramids and the elastomer-CNT composite used to fabricate the piezo-resistive sensors. Plot of frequency output as a function of pressure for an example DiTact sensor. Reprinted with permission from AAAS (Tee et al., 2015).

stretchable networks of mechanical actuators and sensors constructed with nanoribbons of lead zirconate titanate (PZT). The soft PZT sensor-actuator system allows *in vivo* measurements of viscoelasticity in the near-surface regions of the epidermis and also demonstrates broader potential applications including assessment of a variety of pathophysiologic conditions and evaluation of the efficacy of cosmetic products (Dagdeviren et al., 2015a). A skin-inspired artificial mechanoreceptor system using an elastomer-carbon nanotube (CNT) composite structured into microscale pyramids demonstrates the integration of an artificial strain sensor into a biological neural system (Fig. 4**d**). An *in vitro* experiment transferring the broadband (0–200 Hz) output signal from an epidermal strain sensor to the opto-genetically stimulated neurons of a mouse cortex shows the possibility to incorporate strain sensors as a mechanoreceptor for neutral-integrated touch feedback or the potential design of a replacement limb (Tee et al., 2015).

6. Patchable devices for chemical sensing

Body fluids contain various types of ions and small organic molecules. The concentration of these chemicals are valuable parameters for indicating health situation. Skin-patches have been developed to detect the concentration of chemicals such as H^+, Na^+, K^+, Cl^-, lactose and glucose in body fluids (Choi et al., 2017; Gao et al., 2016a; Koh et al., 2016; Martín et al., 2017; Mishra et al., 2017; Wang et al., 2017c). Some chemical sensors also measure the glucose in the blood via diffusion (Bandodkar et al., 2014; Chen et al., 2017). Two representative methods for detection include colorimetry and electrochemical methods.

6.1. Sweat sensing

Sweat is a promising channel to obtain critical information of the biochemical balance of a body in a noninvasive way (Heikenfeld, 2016). One typical method to accurately measure the concentration of chemicals in the sweat is by using the quantitative color change of corresponding indicators followed by a color analysis. An example for such measurement is shown in Fig. 5**a** (Koh et al., 2016). This epidermal sweat sensor consists of four cellulose disks loaded with sensitive reagents for pH, Cl^-, lactose, and glucose, and a surrounding near-field communication (NFC) coil. Soaked with sweat, the color of the disks changes, and the NFC coil activates a nearby smart device, such as a smartphone, which records an image of the device and automatically analyzes the red-green-blue (RGB) components of the indicators, reflecting the concentration of the chemicals. The accuracy of the colorimetric sensors is 0.5 pH units or 0.2, 0.3, and 0.1 mM of Cl^-, lactate, and glucose concentration. The sweat sensors use microfluidic channels typically made of polymeric materials to collect sweat samples, and thereby targets a small quantity from the sample for acquiring effective information. Studies on human sweat show volumetric sweat harvesting rates of ~1.2–12 ml/hour, corresponding to linear filling rates of ~0.07–0.7 mm/min along the microfluidic channels. The reservoirs fill up typically within ~0.3–3.2 h at these sweating rates, with collection time linearly dependent on the reservoir volume. The chemical content of the sweat reflects the health condition, via obtaining information such as concentration of chloride, lactate, pH, glucose, sodium, and potassium, while blood test can usually provide more information on overall and organ-specific health status, but typically requires an invasive or minimally invasive procedure for blood collection (Choi et al.,

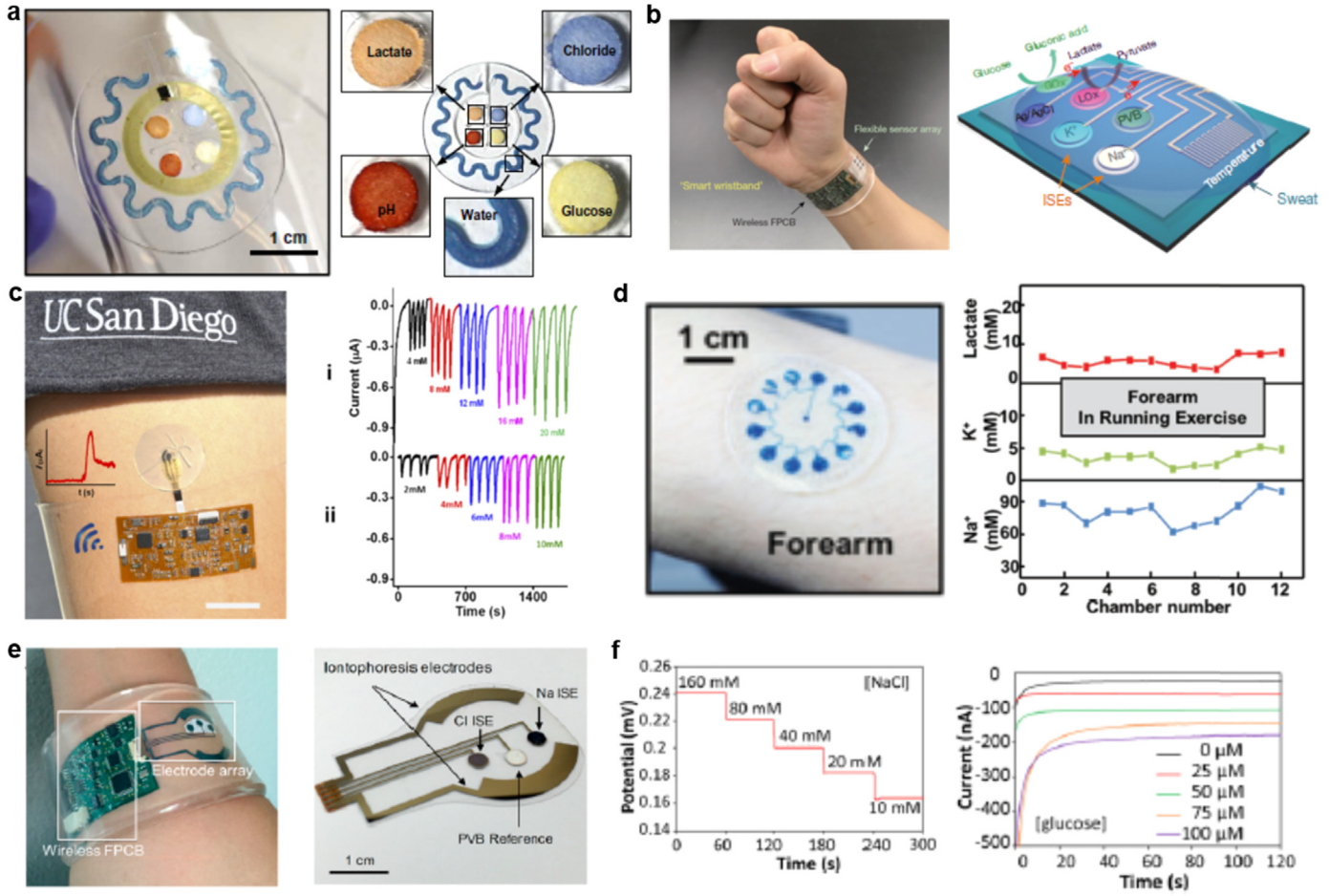

Fig. 5. Wearable sweat biosensor for sensing biochemical species. (a) Left: An epidermal microfluidic biosensor integrated with flexible electronics for sweat monitoring. respective optical images under various mechanical distortions: stretching at 30%strain, bending with 5 cm radius, and twisting. Right: Quantitative colorimetric analysis of markers in sweat. Colorimetric detection reservoirs that enable determination of total water (sweat) loss and concentrations of lactate, glucose, creatinine, pH, and chloride ions in sweat. Reprinted with permission from AAAS (Koh et al., 2016). (b) flexible integrated sensing array for multiplexed perspiration analysis. Left: Photograph of a wearable flexible integrated sensing array on a subject's wrist, integrating the multiplexed sweat sensor array and the wireless flexible printed circuit board. Right: Schematic of the sensor array (including glucose, lactate, sodium, potassium and temperature sensors) for multiplexed perspiration analysis. GOx and LOx, glucose oxidase and lactate oxidase. Reprinted with permission from Nature (Gao et al., 2016a). (c) Microfluidic device design and operation. Left: The soft epidermal microchip device conforms to the skin and routes the sampled sweat toward the electrochemical detector. Photograph of microfluidic device integrated with wireless conformal electronics on skin with lithography-based gold current collectors and screen-printed silver – silver chloride (RE) and Prussian blue (WE and CE). Inset: Electrochemical temporal response to sweat metabolites. Scale bar, 5 mm. Right: Amperometric response for (i) 4, 8, 12, 16, and 20 mM lactate and (ii) 2, 4, 6, 8, and 10 mM glucose at the Prussian Blue enzyme modified electrode. Reprinted with permission from American Chemical Society (Martín et al., 2017). (d) Left: optical images of thin, soft microfluidic devices for chrono-sampling of sweat; Right: In situ chrono chemical analysis of captured sweat samples from forearm during running exercise. Reprinted with permission from Wiley (Choi et al., 2017). (e) Left: A fully integrated wearable sweat extraction and sensing platform (a thin layer of agonist agent hydrogel will be placed underneath the iontophoresis electrodes). Right: Image of iontophoresis and sweat sensor electrodes for Na^+ and Cl^- sensing. (f) Left: The open-circuit potential responses of the sodium using the sensors in NaCl solutions. Right: The chronoamperometric responses of a glucose sensor to glucose solutions. (e), (f) reprinted with permission from National Academy of Sciences (Emaminejad et al., 2017).

2017; Salvo et al., 2010).

Real-time monitoring of the chemical concentration in sweat is enabled by employing electrochemical sensors. Fig. 5**b** illustrates the principle of a sensor system for Na^+, K^+, lactose, and glucose. The alkali metal ions are selectively transduced into electrons, forming an electrochemical cell with the carbon nanotube-based reference electrode, and the electrode potential is measured and converted to the concentration. The organic molecules are oxidized by corresponding enzymes on their electrode, which pairs with an Ag/AgCl standard electrode and the current is also converted to the concentration of ionic species. The accuracy of this electrochemical sensor is about 10 mM for Na^+ and 10 μM for lactose (Gao et al., 2016a). Recent research also reports the detection of other chemicals such as acetone and organophosphate nerve-agents by epidermal electrochemical sensing devices (Mishra et al., 2017; Wang et al., 2017c). Typically, microfluidic channels are used to regulate the flow of sweat as well as to collect sweat for further analysis (Choi et al., 2017; Koh et al., 2016; Martín et al., 2017). In the colorimetric and electrochemical designs, one end of the channel is attached to the skin and the other is open to the air, and the sensor body is located at a chamber in the middle of the channel (Fig. 5**&c**). The flow rate in the channel is controlled by the channel dimensions, and the volume of the collected sweat is monitored by a channel filled with the water-sensitive colorimetric material (Fig. 5**a**).

Chrono-sampling of sweat enabled by a network of microfluidic channels conformally attached to the surface of skin allows historical analysis of the concentrations of key biomarkers, including lactate, sodium, and potassium, thereby offering insights into the overall health status (Fig. 5**d**) (Choi et al., 2017). Another type of sweat biosensors integrates an electrochemically enhanced iontophoresis interface for sweat collection and sensing (Fig. 5**e**). This can be integrated with

cloud-based data analysis technology to enable continuously monitoring of the health status of users with little disturbance and geological constraints (Emaminejad et al., 2017). This platform enables measurement of sodium and chloride levels in sweats, as diagnostic markers for cystic fibrosis, as well as glucose level from iontophoresis-induced sweat for monitoring diabetic conditions (Fig. 5**f**) (Emaminejad et al., 2017).

6.2. Biochemical sensing via photonic techniques

Interaction of light with biological matter yields important information that reflects a certain chemical composition and the associated concentration at the target region. This mechanism enables the possibility of using a wearable photonic system that conformally contacts with the skin to analyze subdermal biochemical conditions in a noninvasive way. Blood oxygenation is a vital indicator for diseases, for organ status, and brain functions. The detection of blood oxygenation using a photonic system typically relies on the absorption difference between red and near-infrared light for oxy- and deoxy hemoglobin. A pulse oximeter based on two organic LEDs (green and red) and an organic polymer photodiode enables high mechanical flexibility for laminating onto soft skin and sufficient photonic sensitivity for detecting hemoglobin-induce absorption (Fig. 6**a**) (Lochner et al., 2014). Such flexible organic optoelectronic systems also show their potential as ultraflexible optoelectronic skins that can both sense oxygenation levels and display information analogically or digitally (Fig. 6**b**) (Yokota et al., 2016). Another example incorporates near-field communication technology with other key photonic components (including LEDs and photodiodes) in a thin flexible form that can be mounted on nearly any position of the body offering wireless operational capability in blood oxygenation sensing with miniaturized device dimensions (Fig. 6**c**) (Kim et al., 2017).

6.3. Blood glucose sensing

Non-invasive sensing of the chemicals in the blood is also achieved by reverse-iontophoresis, i.e. the forced diffusion from the blood plasma to the skin (Bandodkar et al., 2014; Chen et al., 2017). Fig. 6**d** shows a clinically applicable patch where a thin, flexible, and biocompatible paper battery integrated with a gold electrode is adhered on the skin, and the anode drives negatively charged hyaluronate ions deep into the interstitial fluid, increasing the osmotic pressure. As a result, the intravascular glucose is filtered into the interstitial fluid and reaches the skin, and is thus detected electrochemically by electron transfer to glucose oxidase (Chen et al., 2017). Another study uses Ag/AgCl reverse-iontophoresis electrodes (along with the agarose hydrogel coating) for forming a printable skin-worn tattoo platform to efficiently deliver skin interstitial fluid to the working and reference electrodes for electrochemical analysis of glucose concentrations at micromolar levels (Fig. 6**e**) (Bandodkar et al., 2014).

7. Patchable devices for drug/gene delivery

Drug delivery holds another major field that skin-patchable micro-/nano-devices contribute to health care with respect to therapy (Amjadi et al., 2017; Prausnitz and Langer, 2008). Compared with conventional routes, e.g. oral administration or hypodermic injection, the advantages of transdermal patches mainly include: i) controllable drug loading and release- it significantly improves the delivery efficiency and therapeutic performance; ii) bio-safety- most patchable transdermal devices use insulated microchannels to relieve the risk of disease transmission in the procedure of drug loading; iii) minimum invasiveness- micro-/nano-fabrication technology miniaturizes the surface of the delivery regions (e.g. tips of microneedles) in contact with the nerve system in deeper layer, thus remarkably relieving the risk of infections and pains as compared to hypodermic needles.

Since the first approval for clinical use, the transdermal delivery system has undergone three generations (Prausnitz et al., 2004). The first-generation systems were mostly drug-loaded patches which relied on passive molecular diffusion across the stratum corneum. The transport efficacy was limited to the size and solubility of the cargo (e.g. lipophilic small drugs). The second generation was supplied with external stimuli, e.g. chemical enhancer or physical approaches, to improve drug diffusion efficiency through the skin. These methods easily lead to skin damage or irritation associated with external enhancement. The third generation of transdermal devices adopted microneedles or an integrated micro-actuation system to actively diffuse cargo molecules under the epidermis. The applications have been largely extended to macromolecular drugs or vaccines.

Skin-patchable transdermal devices are now considered as the fourth-generation (Lee et al., 2016a). Advances in flexible electronics have allowed the devices to integrate a variety of functions on one chip (Lee et al., 2017). The devices are applied for on-skin sensing as summarized above. A growing number of pioneering research in recent years scaled the device down to nanometer sizes, achieving unprecedented functionalities. For instance, a novel nano-transfection device that can directly 'shoot' naked large-molecular-plasmids into epidermal cells has overcome the limitations of previous devices on transcellular gene delivery (Gallego-Perez et al., 2017). This breakthrough shows promise in skin-based gene therapy with an expectation for in-body regenerative medicine. Excellent reviews focusing on transdermal delivery have been provided following the three generations of devices (Lee et al., 2017; Prausnitz, 2004; Prausnitz and Langer, 2008). In this section, depending on either intracellular or extracellular transport, we classify the devices into two categories, i.e. transdermal local delivery and direct intracellular gene delivery.

7.1. Transdermal local delivery

Transdermal local delivery devices aim to overcome the barrier of the stratum corneum (the outer most layer of skin) and deliver the cargo (e.g. drugs) into the epidermis or dermis (Paudel et al., 2010). Most techniques categorized in the three generations can be defined as 'local' delivery devices. The cargo, in these themes, mostly are small molecules such as hydrophilic drugs, or chemical vectors modified genes (e.g. liposome, polyplex, peptides) that can easily be taken up by cells, (Prausnitz and Langer, 2008). These devices are not specifically designed to penetrate epidermal or dermal cells. Skin patchable devices for this objective have been realized through a variety of mechanical approaches, i.e. microneedles.

The inception of manufacturing microneedles on silicon was realized with the development of microelectromechanical system (MEMS) techniques (Henry et al., 1999; McAllister et al., 2003; Moh et al., 2009). Deep reactive ion etching, laser cutting, and photolithographic methods were implemented to obtain the targeted size and spacing between microneedles in a microneedle patch (Prausnitz, 2017). For decades, silicon microneedles have provided obvious advantages for bio-application, such as high-throughput, dimensional control, batch production and compatibility with an integrated system (Donnelly et al., 2010; Prausnitz, 2004). These solid needles are generally used to pierce the skin, and create pathways for drug diffusion, often referred to as the "poke and patch" approach (Chege et al., 2017; Sanjay et al., 2018). Two noticeable limitations of solid microneedles for drug delivery include non-biodegradability and the issues on self-healing of the skin (Sanjay et al., 2018). Chemical-/bio-coating of microneedles with drugs or fabrication of hollow microneedles with drug reservoirs were reported later for the sake of delivery efficiency and bio-safety (Chege et al., 2017).

The silicon chip is rigid and brittle, becoming unfavorable to skin adjustment, thus being replaced by polymeric flexible microneedles. Depending on the purpose, polymeric needles can be made by using dissolvable (e.g. dextran, gelatin, polyvinylpyrrolidone [PVP], etc),

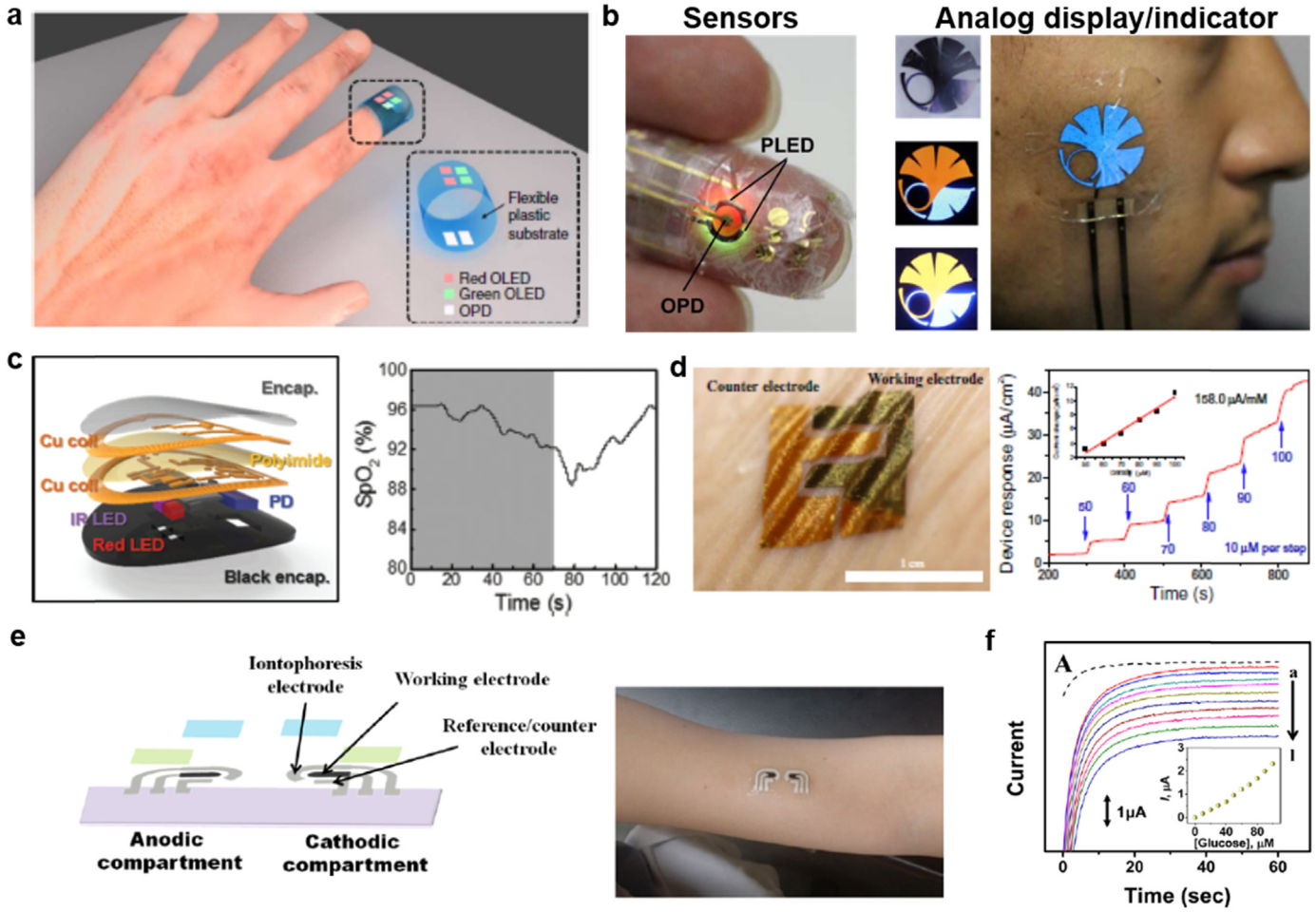

Fig. 6. Wearable photonic microdevices for biochemical sensing on skin. (a) Organic optoelectronic sensor for pulse oximetry. Pulse oximetry sensor is composed of two OLED arrays and two OPDs. Reprinted with permission from Nature Publishing Group (Lochner et al., 2014). (*b)* Smart e-skin system comprising health-monitoring sensors, displays, and ultraflexible PLEDs. Reprinted with permission from AAAS (Yokota et al., 2016). (c) millimeter-scale, NFC enabled pulse oximeter device. Calculated SpO2 based on measurements of the device during breath hold test showing a visible drop in oxygen saturation. Reprinted with permission from Wiley (Kim et al., 2017). (d) Electrochemical twin channels principle and the skin-like biosensors. Left: Selective electrochemically deposited dual electrodes of the biosensors. The biosensor completely conforms to the skin surface. Right: moderate-density glucose as measured in a calibration experiment. (Inset) Biosensor response as a function of density. Reprinted with permission from AAAS (Chen et al., 2017). (e) Tattoo-based platform for noninvasive glucose sensing. Left: Schematic of the printable iontophoretic-sensing system displaying the tattoo-based paper (purple), Ag/AgCl electrodes (silver), Prussian Blue electrodes (black), transparent insulating layer (green), and hydrogel layer (blue). Middle: Photograph of a glucose iontophoreticsensing tattoo device applied to a human subject. Right: Chronoamperometric response of the tattoo-based glucose sensor to increasing glucose concentrations from 0 μM (dashed) to 100 μM (plot "l") in buffer in 10 μM increments. Reprinted with permission from American Chemical Society (Bandodkar et al., 2014).

swellable (e.g. polyvinyl alcohol [PVA], acrylate modified HA, polyethylene glycol [PEG], etc) and biodegradable (e.g. polylactic acid [PLA], polyglycolic acid [PGA], polycarbonate, chitin, etc) polymers (Wang et al., 2017d). These microneedles are either coated or loaded with drugs, the former being commonly used. Two issues should be considered in design of microneedles: how to poke and create a path for drug delivery, and how to release the drug from the encapsulation underneath the skin (Prausnitz, 2017).

The latest research studies adopting polymeric devices typically are designed for vaccination and insulin injection (Kim and Meng, 2016; Kim et al., 2012). DeMuth et al. (2013) reported a poly(l-lactide) microneedle for DNA vaccine delivery (Fig. 7**a**). Polyelectrolyte multilayers (PBAE/pDNA polyplex) were coated on the microneedles (650 μm in height, 250 μm in diameter) using layer-by-layer (LbL) deposition (Fig. 7**b**). The PLLA microneedle is biocompatible and bioabsorbable, forming an ideal substrate for skin patches in clinical trials. The multilayers of PBAE allow for sustainable release of pDNAs. *Ex vivo* experiments with the skin of rhesus macaques showed that the microneedle regimen with multilayers generated long-term, consistent expression of transfection by delivery of poly-1/Pluc (Fig. 7**c**). A polyvinylpyrrolidone (PVP) microneedle (650 μm in height, 10 μm radius) encapsulating the inactivated influenza vaccine was developed for local vaccination (Fig. 7**d and e**) (Sullivan et al., 2010). Serial *in vivo* mice experiments, including antigen stability, humoral/recall immune response, and cytokine response, demonstrated that the flexible microneedle provided more efficient virus immunization and cellular recall responses, as compared to traditional intramuscular vaccination (Fig. 7**f**). Microneedles made with photoresists (e.g. SU-8), polyvinyl alcohol (PVA) and sucrose were co-assembled onto a soft substrate. Integrated with a self-powered system, the wearable device has potential for clinical trials for long-term transdermal insulin delivery (Fig. 7**g, h**) (Wang et al., 2016a). Besides, a contact-free, electro-drawing method was recently introduced to implement poly (lactic-*co*-glycolic acid) (PLGA) biodegradable microneedles for delivery of bioactive agents into hypodermic tissues. A flexible array of microneedles (inner diameter: 500 μm) was manufactured on PDMS substrate by electro-drawing force under an electric field (Fig. 7**i**) (Vecchione et al., 2014). Preliminary experiments on animal skin confirmed the

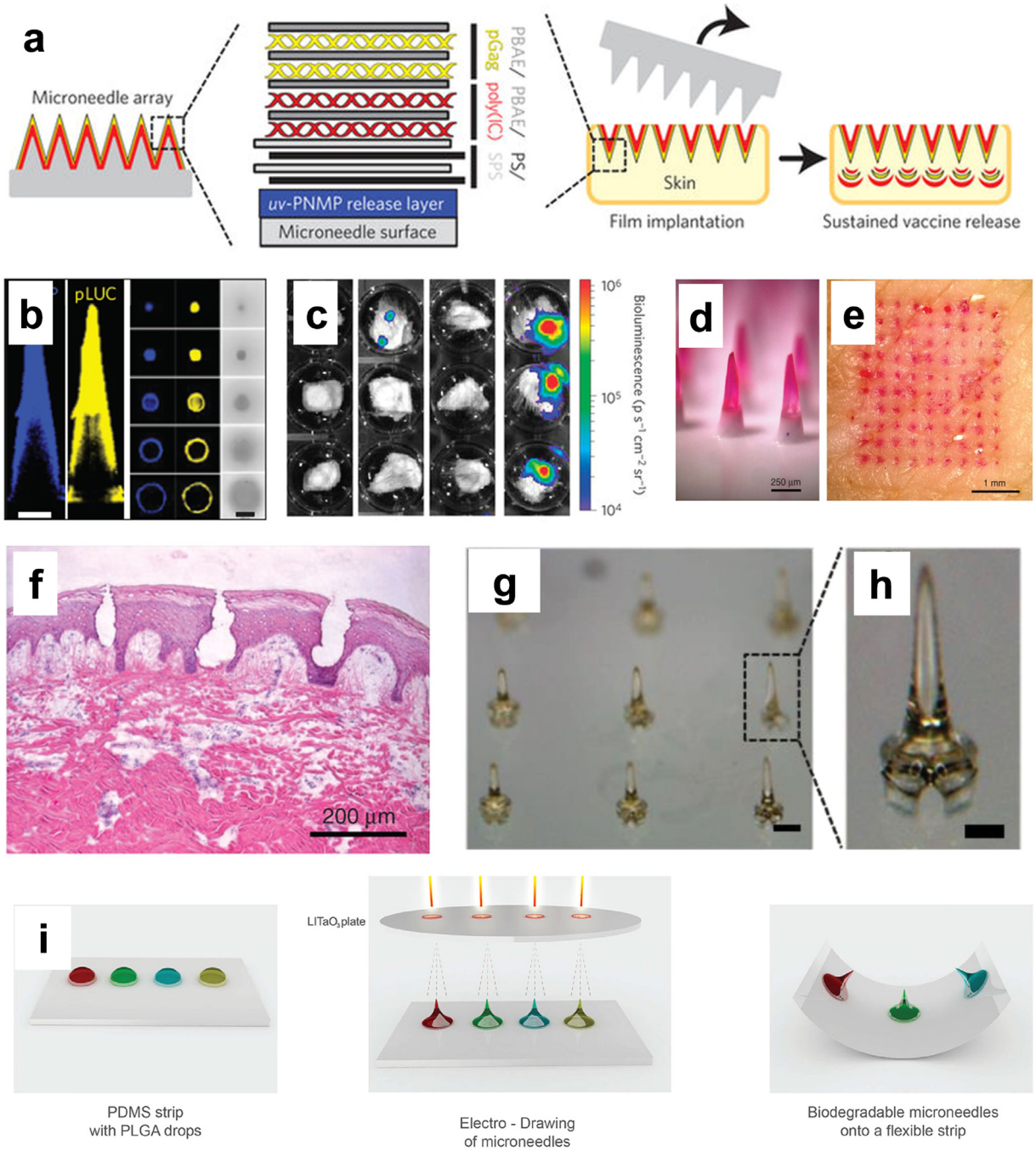

Fig. 7. Wearable flexible transdermal needle devices for local delivery of drugs and vaccines across stratum corneum. (a) Silicon templated flexible poly(l-lactide) microneedle for DNA vaccine delivery. Multiple layers of electrolytes (e.g. PBAE) sandwiching cargo (e.g. vaccine, pGag, poly(lC)) by lbl deposition, allowing for sustainable cargo release. (b) confocal images of PLLA microneedles coated with (SAv488-bPNMP)(PS/SPS)20(poly-1/Cy5-pLUC)35 films. (c) Bioluminescence images of luciferase expression 2 days after pLUC delivery by ID injection or microneedle. Reproduced with permission from Nature (DeMuth et al., 2013). (d) Dissolvable PVP microneedles encapsulated with influenza vaccine. (e) Porcine skin after piercing and removal of microneedles, showing the delivery of sulforhodamine. (f) The cross-section of the skin penetrated with microneedles. Reproduced with permission from Nature (Sullivan et al., 2010). (g) and (h) A PVA and sucrose coated SU-8 microneedle system has been implemented for long-term insulin transdermal delivery. Reproduced with permission from Wiley (Wang et al., 2016a). (i) The schematic of the PLGA biodegradable microneedle fabrication on a flexible substrate using electro-drawing method. Reproduced with permission from Wiley (Vecchione et al., 2014).

feasibility of the needle on local delivery of small molecular dyes.

Besides the needle patch, ultra-sound working at a wide range of frequencies from 20 kHz to 16 MHz have also been adopted for transdermal drug delivery, known as 'sonoporation' (Marx, 2015; Mitragotri, 2005). Typically, lower frequencies (< 100 kHz) can generate transient pores in the membrane for effective sonophoresis, which facilitates the movement of the cargo in the procedure of transdermal delivery (Mitragotri et al., 1995; Mitragotri and Kost, 2004). *In vivo* applications were mainly achieved by using ultra-sound to guide microbubbles-enhanced sonoporation (Yuana et al., 2017). The biophysical mechanism of drug delivery into the cell using microbubble-assisted ultrasound has been studied, by a transducer and a signal generator to deliver pEGFP into human lymphoma cells and captured real time images using a high speed camera (Nejad et al., 2016). Another research proved successful

administration of doxorubicin (DOX, an anticancer drug) into breast cancer cell lines without the use of microbubbles. The ultrasonic setup using piezo-ceramic focused transducers, a hydrophone and a waveform generators have made the dynamics of cell permeabilization more controllable for drug dose control while reducing the side effects of the ultrasound (Chettab et al., 2017). However, pushing sonoporation toward clinical skin-patch is hampered by the challenges in the miniaturization of ultrasound generators. Recently, Zhang et al. reported a portable, hypersonic poration system for local gene and drug delivery, which shows a possibility of patchable sonoporation for *in vivo* trials (Zhang et al., 2017b).

7.2. Direct intracellular delivery

The latest research breakthrough, including gene editing, cell reprogramming, and adoptive immunotherapy, relies on directly introducing gene materials (e.g. DNAs, RNAs) into cells (Ganta et al., 2008; Prausnitz and Langer, 2008). In fact, most engineered cargo in these scenarios, such as reprogramming factors (Gonzalez et al., 2011), CRISPR-Cas9 (Konermann et al., 2015; Shalem et al., 2014), chimeric antigen receptor (CAR) plasmids (Levine, 2015), face extreme challenges in the efficiency of cellular internalization due to their large molecular weights (> 6 kbps). Local transdermal vehicle systems, relying on molecular diffusion at the endpoint, lead to low efficiency and limited throughput in transporting naked DNAs and proteins (Adam Seger et al., 2012; Boukany et al., 2011; King, 2004; Mehier-Humbert and Guy, 2005). Physically, precise transporting macromolecules into cells requires the device or functional zone be significantly smaller than the cell, often in nanoscales (Boukany et al., 2011; Henslee et al., 2011). The delivery pathway needs to be precisely manipulated over the cell membrane (Chang et al., 2016a). The Lee group recently reported a nano-patch system which could directly transfect reprogramming transcriptional factors into epidermal and dermal cells for 'in-patient' skin reprogramming (Fig. 8**a**) (Gallego-Perez et al., 2016; Gallego-Perez et al., 2017). The patchable device had an array of nanochannels etched through the silicon wafer. In tight contact with the skin of the mouse, the nanochannel was aligned onto epidermal cells (Fig. 8**b**). The nanochannel-assisted electroporation precisely optimized the potential drop across the cell membrane for safe electroporation while 'electrophoretically' drives large-molecular weight transcriptional factors into epidermal cells for *in vivo* cell reprogramming (Chang et al., 2016b). Deep reprogramming of dermal cells via internal propagation of extracellular vesicles (EVs) was also observed upon the skin electrotransfection. The team successfully reprogrammed skin cells into induced endothelial cells (iECs) by delivery of defined transcriptional factors, Etv2, Foxc2, Fli1 (EFF) (Fig. 8**c**). By this way, the nano-patch demonstrated wound healing of the whole limb based on cell reprogramming. On-skin delivery of EFF factors resulted in re-establishment of blood vessel streams while improving the blood perfusion as early as 7 days after treatment (Fig. 8**d**). This was the first study in which a patchable nanodevice for rapid and non-invasive delivery of reprogramming factors into the skin.

For clinical therapy, *in vivo* reprogramming has shown effectiveness by using available cell sources from the same patient, which circumvents the issues associated with *ex vivo* processing. However, current reprogramming methods relying on viral and chemical transfection would cause noticeable side-effects due to long circulation. The skin-patchable delivery device, in contrast, shows a simple approach for local, topical reprogramming of dermal cells into other somatic cells. In addition, this device initiates the paradigm of a 3D nanochannel array device for high-throughput gene delivery *in vitro* and *in vivo* (Prausnitz et al., 2004; VanDersarl et al., 2012; Wei et al., 2014; Wu et al., 2015b; Xie et al., 2012). A soft electroporation device based on gold hollow nanoelectrodes was fabricated on a PDMS membrane (Fig. 8**e**) (Caprettini et al., 2017). The Li group reported a flexible microneedle electroporation array for *in vivo* DNA and siRNA delivery into mouse skin (Wei et al., 2014). Silicon needles were implemented on a parylyene membrane, showing promising bendability. To subsidize the fabrication cost, the group proposed another device adopting a microneedle roller and a flexible interdigitated electroporation array (FIEA) (Huang et al., 2018). A microneedle roller is used to disrupt the skin and create liquid paths, thereby facilitating it as a liquid electrode while FIEA is used as a pliable substrate for tight contact with the skin as well as it helps in generation of an even electric field. Another benefit of this device is the promising cell safety due to low voltage. Patching the device on mouse skin successfully injected the RFP expressing gene and siRNA into epithelial cells.

Laser is another type of physical capability for ablating the stratum corneum. Transdermal laser delivery has been commercialized for macromolecules and vaccinations. Wu et al. reported a nanochannel array chip based on silicon dioxide which can focus an external laser source onto a tiny spot on tissue or cells (Fig. 8**f**) (Wu et al., 2015b). In another research, microbubbles were produced by a microsecond laser system to administer FITC and plasmids into NIH/3T3 cells (Fan et al., 2015). Via the laser-induced membrane poration, large molecules, even bacteria, could be administered into cells. Similar to sonoporation, the laser system is difficult for miniaturization of laser sources for a skin-patchable device.

Beside electroporation, another prototype claiming direct cellular delivery of cargoes are based on nanoneedles. Various non-degradable (semiconducting nanowires, carbon nanotubes/nanofibers) and biodegradable (porous Si) materials for nanoneedles have been reported (Chiappini et al., 2015b). Recently, a non-degradable carbon nanosyringe arrays (CNSAs) platform are reported for cargo delivery. These carbon nanosyringes possessed hollow nanotubes which were loaded with desired cargoes in aqueous solution. The team delivered plasmids (pEGFP) and quantum dots via diffusion into NIH3T3 and human mesenchymal stem cells (hMSCs) *in vitro*, yet not conducted on animal model (Park et al., 2009). A diamond nanoneedle array was reported (Fig. 9**a**) to disrupt the cell membrane and to have a high throughput intracellular delivery. The diamond nanoneedles with heights varying from 200 nm to 1.3 μm and a tip radius of 10 nm was fabricated by using the bias-assisted reactive ion etching of a diamond deposited silicon substrate (Zhu et al., 2015). A luminescent iridium (III) polypyridine complex and cisplatin were used to demonstrate the effectiveness of diamond nanoneedles for intracellular delivery (Fig. 9**b**) (Yan et al., 2014). Biodegradable nanoneedles have gained more attention owing to their cytocompatibility properties. Biodegradable porous Si has been fabricated into nanoneedles for drug delivery, based on chemical etching, photolithography, and reactive ion etching (Chiappini et al., 2015b). *In vivo* verification of drug delivery was carried out by injecting quantum dots into the skin cells of a mouse. Focused ion beam-scanning electron microscopy (FIB-SEM) showed that the nanoneedles were in tight contact with the cytosol. The nanoneedles' degradation was observed after 15 h from injection time. The same team also reported using biodegradable silicon nanoneedles (Fig. 9**c**) to deliver nucleic acids intracellularly to induce *in vivo* neovascularization (Chiappini et al., 2015a). The efficacy of these nanoneedles was measured by co-delivering Cy3-labelled GAPDH siRNA and GFP expressing DNA plasmid and assessing GFP expression and siRNA fluorescence (Fig. 9**d**). Furthermore, microinjection and nanoneedle injection were compared by injecting the same amount of VEGF plasmid into the muscle cells of mice, and the results showed *in vivo* nanoinjection device successfully induced neovascularization with high blood perfusion (Chiappini et al., 2015b).

Free-standing single-walled carbon nanotubes (SWCNTs) and gold nanorods (GNRs) have also been used as nanoneedles to directly deliver genes/drug into nucleus rather than cytosol, which show potentials to design skin patches by aligning and assembling SWCNTS or GNRs on a flexible substrate. CNTs possessed intrinsic optical and physical characteristics, thereby adding an optical imaging technique during drug delivery (Boyer et al., 2016). In a recent work, SWCNTS were non-

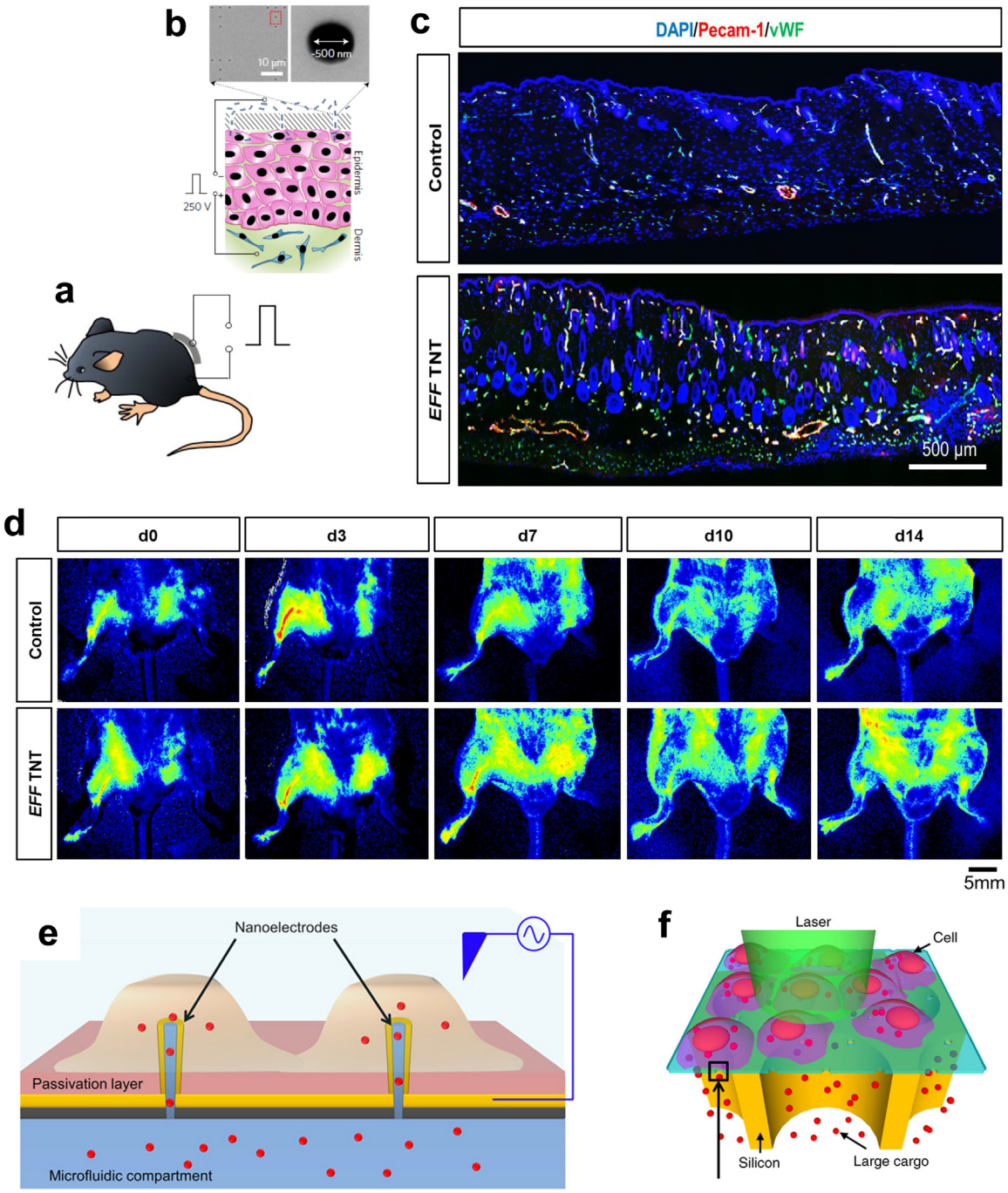

Fig. 8. Nano-patch devices for direct delivery of drugs and vaccines into skin cells *in vivo*. (a) A nanochannel electroporation chip is patched on mouse skin for epidermal gene delivery. (b) The nanochannel fabricated on silicon chip allows for precise cell-electroporation while dose-control for delivery of large molecular weight transcriptional factors. (c) successful epidermal and dermal cells reprogramming into induced endothelial cells (iEC) in mouse skin by delivery of defined transcriptional factors (EFF factors), as demonstrated with immunostaining with endothelial marker, Pecam-1 and vWF. (d) whole limb blood vessel rescue by simple delivery of EFF factors using nano-delivery patch. Reproduced with permission from Nature (Gallego-Perez et al., 2017). (e) A flexible nano-electroporation with potential for patching on skin. Reproduced with permission from Nature (Caprettini et al., 2017). (f) A laser system for precise gene delivery into cells via nanochannel array chip. Reproduced with permission from Nature (Wu et al., 2015b).

covalently attached with the tail domain of the nuclear protein lamin B1 (LB1) or Bovine Serum Albumin (BSA). The cellular and nuclear nuclealization of SWCNTs and LB1 or BSA were verified and molecular interaction between SWCNTs-BSA and SWCNTs-LB1 and DNA within the nucleus was measured (Fig. 9**e**). Cysteamine (Cys) was functionalized with GNRs to attach folic acid (FA) and Doxorubicin (DOX), an anti-cancer drug for targeting and treating cancer (Pandey et al., 2013). Another team utilized polydopamine (PDA) capped polyethylene glycol (PEG) grafted GNRs to attach the drugs (Methylene Blue (MB) and DOX) for Hela cells inhibition (Fig. 9**f**) (Wang et al., 2016b).

8. Conclusions and future perspective

Skin patchable devices are drawing increasing attentions among biomedical devices as the skin is an ideal and easily accessible organ reflecting internal environments of the body. Novel processing

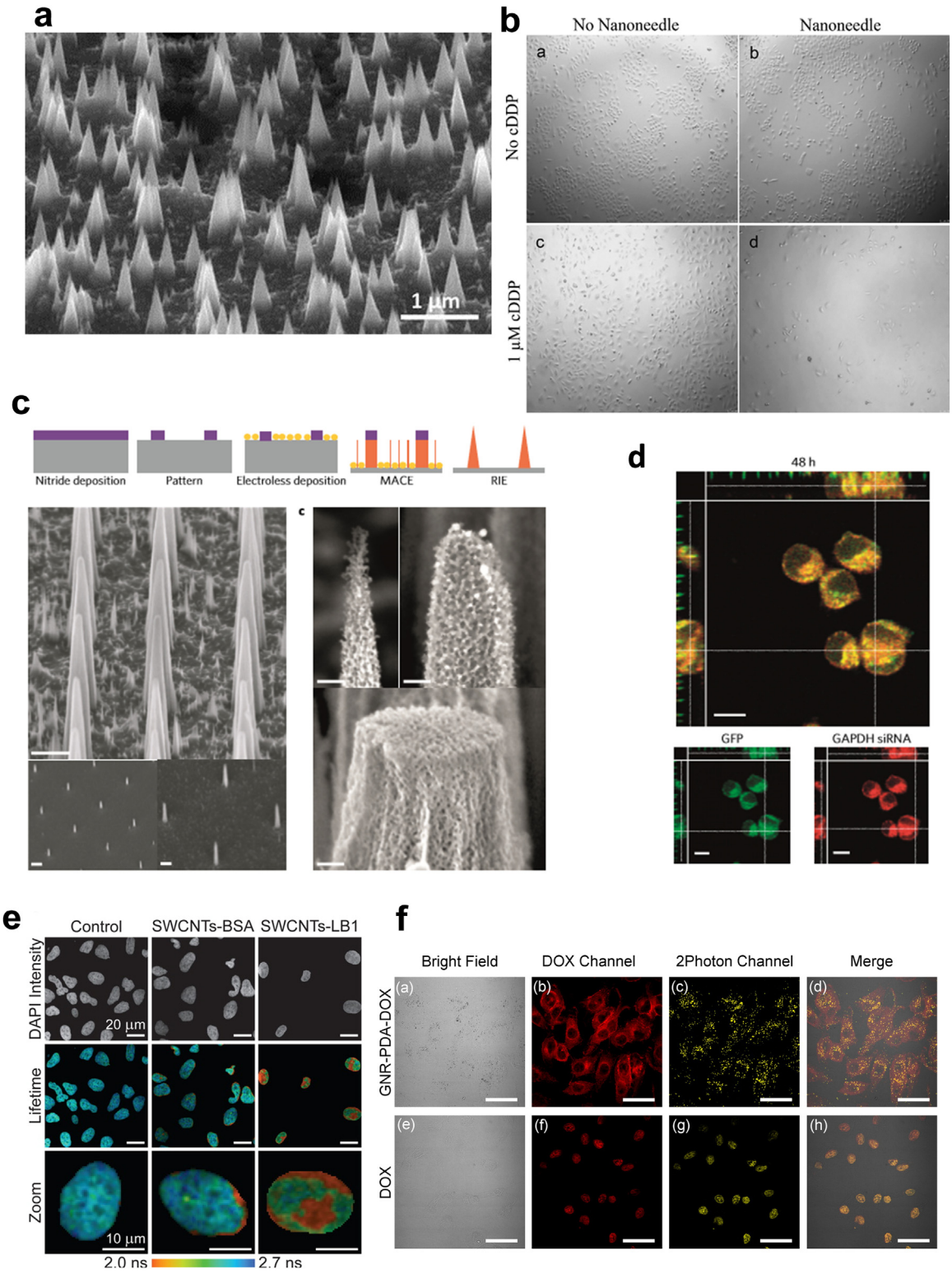

Fig. 9. Nanoneedles for intracellular delivery. (a) SEM image of diamond nanoneedle arrays. Reproduced with permission from Springer (Zhu et al., 2015). (b) Bright-field images of cells delivered with cisplatin treated with diamond nanoneedle 72 h post plating. Reproduced with permission from Wiley (Yan et al., 2014). (c) Porous silicon nanoneedles synthesis combining conventional microfabrication and metal-assisted chemical etch (MACE). (d) Intracellular co-delivery of nucleic acids such as GAPDH-siRNA (Cy3 labelled in yellow) and GFP plasmid (GFP in green) to cells in culture after application using the nN-B interfacing strategy. Confocal image acquired 48 h post transfection. The siRNA and GFP signal are present diffusely throughout the cytosol. Scale bars, 5 μm. Reproduced with permission from Nature (Chiappini et al., 2015a). (e) Free-standing nanoneedles show potential skin patchable devices for drug delivery based on SWCNTs–BSA for HeLa cells treatment. Reproduced with permission from ACS (Boyer et al., 2016). (f) Gold nanorods (GNRs) modified PDA-DOX nanocomposites used for Hela cells treatment. Scale bars, 50 μm. Reproduced with permission from ACS (Wang et al., 2016b).

approaches with new materials and their combinations have created potentials for integrating biosensors, microfluidics, even an integrated lab-on-chip systems toward clinical use. Unconventional skin-patchable devices exhibit capabilities in capturing essential physiological signals outward and delivering molecules inward at epidermal interfaces. The miniaturized physical dimension, weight and high mechanical flexibility provide skin-patchable devices with better interfaces with users. Furthermore, aims for more sophisticated and comprehensive manipulation of skin micro-environments essentially intrigue wide participation in the research field.

In this review, we summarized advances in skin patchable micro-/nano-devices for electrical, thermal, mechanical, and chemical sensing and gene delivery purposes along with the materials used for the device fabrication. Direct electrical contact and capacitive-coupled sensors establish two promising routes for electrical sensing. Thermal sensing based on temperature modulation in electrical resistance or photonic property enables detection of essential medical diagnostic references. Patchable mechanical sensors not only exhibit monitoring capability in whole body motion but also offer more localized sensing function for certain epidermal diseases. Chemical sensing from skin prevents risks in discomfort, and possible irritation during invasive contact with biochemical and tissue and provides insights on the physiological status that reflects certain inner organs and whole metabolic systems. Existing commerialized patchable sensors including BioStamp of MC10, VitalPatch of VitalConnect, Sweatronics of Eccrine Systems, and NFC and Optical Skin Patches of GENTAG, target on improving personal heathcare, medical monitoring and atheletic or fitness training. Waterproof capability, wireless communication, high sensing precision, and long-term usage (via rechargeable battery or battery-free technology) highlight many of those commercialized skin-patchable devices (Boroojerdi et al., 2017; Cohen, 2008; Heikenfeld et al., 2018; Kabir et al., 2017; Selvaraj, 2015). Future efforts in patchable biosensors have shown trends in four fronts: i) introduction of advanced materials for enhanced performance and skin-interfacing; ii) the developments of fabrication techniques that enable industry-level reliability and low cost; iii) data collection strategies (e.g. wireless technology) and analysis algorithms that maximize full potential of biosensors and provides essential and accurate information with high efficiency; iv) integration and compatibility with existing clinical means in a way that can readily be adopted by users without compromising other accustomed clinical techniques.

Transdermal drug delivery patches have been established for decades. This paradigm attracted numerous researches due to their advantages of control-release, biocompatibility, and minimum invasiveness. Among the first three generations of transdermal devices, silicon microneedles were gradually replaced by soft and flexible polymeric microneedles. New demos of single cell physical-poration platforms have been implemented in transdermal delivery devices. The next generation of transdermal nanodevices focus on extending the delivery to macromolecular drugs, naked DNAs, genes, composites, and those facing challenges in transportation across the cell membrane of the epidermis or dermis. A recent breakthrough reports one possibility of using single cell nano-electroporation to facilitate direct transfection of large reprogramming plasmids into the epidermis, and dermis. Future innovations of these nanotechnologies are expected to assemble system level device for more user-friendly manipulations. In addition, another possibility is to target an internal body, e.g. organ gene delivery patches. Direct transferring macromolecules holds greater promises in the genetic engineering field by reprogramming cells *in vivo* to correct genetic mutation or to treat a genetic disease. Nevertheless, investigating and implementing new materials to fabricate devices always aids in accelerating the research and development for clinical testing and validation.

Acknowledgements

L. Chang thanks the start-up and RSG funds of UNT. T. Kuang acknowledges the financial support of National Natural Science Foundation of China (No. 51803062), Natural Science Foundation of Guangdong Province of China (No. 2018A030310379), National Postdoctoral Program for Innovation Talents (No. BX201700079), China Postdoctoral Science Foundation Funded Project (No. 2017M620371), and Foundation for Distinguished Young Talents in Higher Education of Guangdong Province (No. 2017KQNCX001). R. Yang acknowledges the funding from the Nebraska Center for Integrated Biomolecular Communication (NCIBC) (NIH National Institutes of General Medical Sciences P20 GM113126).

References

Adam Seger, R., Actis, P., Penfold, C., Maalouf, M., Vilozny, B., Pourmand, N., 2012. Nanoscale 4 (19), 5843–5846.
Amjadi, M., Mostaghaci, B., Sitti, M., 2017. Curr. Gene Ther. 17 (2), 139–146.
Axisa, F., Vanfleteren, J., Vervust, T., 2012. Method for manufacturing a stretchable electronic device. Google Patents.
Banaee, H., Ahmed, M.U., Loutfi, A., 2013. Sensors 13 (12), 17472–17500.
Bandodkar, A.J., Jia, W., Yardımcı, C., Wang, X., Ramirez, J., Wang, J., 2014. Anal. Chem. 87 (1), 394–398.
Bartlett, M.D., Markvicka, E.J., Majidi, C., 2016. Adv. Funct. Mater. 26 (46), 8496–8504.
Bonato, P., 2003. IEEE Eng. Med. Biol. 22 (3), 18–20.
Bonato, P., 2010. IEEE Eng. Med. Biol. 29 (3), 25–36.
Boroojerdi, B., Claes, K., Ghaffari, R., Mahadevan, N., Markowitz, M., Melton, K., Morey, B., Otoul, C., Patel, S., Phillips, J., 2017. Movement Disorders. Wiley 111 River St, Hoboken.
Boukany, P.E., Morss, A., Liao, W.C., Henslee, B., Jung, H., Zhang, X., Yu, B., Wang, X., Wu, Y., Li, L., Gao, K., Hu, X., Zhao, X., Hemminger, O., Lu, W., Lafyatis, G.P., Lee, L.J., 2011. Nat. Nanotechnol. 6 (11), 747–754.
Boyer, P.D., Ganesh, S., Qin, Z., Holt, B.D., Buehler, M.J., Islam, M.F., Dahl, K.N., 2016. Delivering single-walled carbon nanotubes to the nucleus using engineered nuclear protein domains. ACS Appl. Mater. Inter 8 (5), 3524–3534.
Caprettini, V., Cerea, A., Melle, G., Lovato, L., Capozza, R., Huang, J.A., Tantussi, F., Dipalo, M., De Angelis, F., 2017. Sci. Rep. 7, 8524.
Chang, L., Bertani, P., Gallego-Perez, D., Yang, Z., Chen, F., Chiang, C., Malkoc, V., Kuang, T., Gao, K., Lee, L.J., Lu, W., 2016a. Nanoscale 8 (1), 243–252.
Chang, L., Gallego-Perez, D., Chiang, C.L., Bertani, P., Kuang, T., Sheng, Y., Chen, F., Chen, Z., Shi, J., Yang, H., Huang, X., Malkoc, V., Lu, W., Lee, L.J., 2016b. Small 12 (43), 5971–5980.
Chege, M., McConville, A., Davis, J., 2017. J. Chem. Health Saf. 24 (2), 6–14.
Chen, Y., Lu, S., Zhang, S., Li, Y., Qu, Z., Chen, Y., Lu, B., Wang, X., Feng, X., 2017. Sci. Adv. 3 (12), e1701629.
Chettab, K., Mestas, J.L., Lafond, M., Saadna, D.E., Lafon, C., Dumontet, C., 2017. Mol. Pharm. 14 (2), 441–447.
Chiappini, C., De Rosa, E., Martinez, J.O., Liu, X., Steele, J., Stevens, M.M., Tasciotti, E., 2015a. Nat. Mater. 14 (5), 532–539.
Chiappini, C., Martinez, J.O., De Rosa, E., Almeida, C.S., Tasciotti, E., Stevens, M.M., 2015b. ACS Nano 9 (5), 5500–5509.
Choi, J., Kang, D., Han, S., Kim, S.B., Rogers, J.A., 2017. Adv. Healthc. Mater. 6 (5), 1601355.
Chu, H., Jang, H., Lee, Y., Chae, Y., Ahn, J.-H., 2016. Nano Energy 27, 298–305.
Chun, K.Y., Oh, Y., Rho, J., Ahn, J.H., Kim, Y.J., Choi, H.R., Baik, S., 2010. Nat. Nanotechnol. 5 (12), 853–857.
Cohen, M.H., 2008. One point calibration integrated temperature sensor for wireless radio frequency applications. Google Patents.
Dagdeviren, C., Shi, Y., Joe, P., Ghaffari, R., Balooch, G., Usgaonkar, K., Gur, O., Tran, P.L., Crosby, J.R., Meyer, M., 2015a. Nat. Mater. 14 (7), 728–736.
Dagdeviren, C., Shi, Y., Joe, P., Ghaffari, R., Balooch, G., Usgaonkar, K., Gur, O., Tran, P.L., Crosby, J.R., Meyer, M., Su, Y., Chad Webb, R., Tedesco, A.S., Slepian, M.J., Huang, Y., Rogers, J.A., 2015b. Nat. Mater. 14 (7), 728–736.
DeMuth, P.C., Min, Y.J., Huang, B., Kramer, J.A., Miller, A.D., Barouch, D.H., Hammond, P.T., Irvine, D.J., 2013. Nat. Mater. 12 (4), 367–376.
Deng, B., Hsu, P.-C., Chen, G., Chandrashekar, B., Liao, L., Ayitimuda, Z., Wu, J., Guo, Y., Lin, L., Zhou, Y., 2015. Nano Lett. 15 (6), 4206–4213.
Donnelly, R.F., Singh, T.R.R., Woolfson, A.D., 2010. Drug Deliv. 17 (4), 187–207.
Dul, M., Stefanidou, M., Porta, P., Serve, J., O'Mahony, C., Malissen, B., Henri, S., Levin, Y., Kochba, E., Wong, F., 2017. Hydrodynamic gene delivery in human skin using a hollow microneedle device. J. Control Release 265, 120–131.
Emaminejad, S., Gao, W., Wu, E., Davies, Z.A., Nyein, H.Y.Y., Challa, S., Ryan, S.P., Fahad, H.M., Chen, K., Shahpar, Z., 2017. Proc. Natl. Acad. Sci. USA 114 (18), 4625–4630.
Fan, Q., Hu, W., Ohta, A.T., 2015. Lab Chip 15 (2), 581–588.
Gallego-Perez, D., Otero, J.J., Czeisler, C., Ma, J., Ortiz, C., Gygli, P., Catacutan, F.P., Gokozan, H.N., Cowgill, A., Sherwood, T., Ghatak, S., Malkoc, V., Zhao, X., Liao, W.C., Gnyawali, S., Wang, X., Adler, A.F., Leong, K., Wulff, B., Wilgus, T.A., Askwith, C., Khanna, S., Rink, C., Sen, C.K., Lee, L.J., 2016. Nanomedicine 12 (2), 399–409.
Gallego-Perez, D., Pal, D., Ghatak, S., Malkoc, V., Higuita-Castro, N., Gnyawali, S., Chang,

L., Liao, W.C., Shi, J., Sinha, M., Singh, K., Steen, E., Sunyecz, A., Stewart, R., Moore, J., Ziebro, T., Northcutt, R.G., Homsy, M., Bertani, P., Lu, W., Roy, S., Khanna, S., Rink, C., Sundaresan, V.B., Otero, J.J., Lee, L.J., Sen, C.K., 2017. Nat. Nanotechnol. 12 (10), 974–979.
Ganta, S., Devalapally, H., Shahiwala, A., Amiji, M., 2008. J. Control Release 126 (3), 187–204.
Gao, W., Emaminejad, S., Nyein, H.Y.Y., Challa, S., Chen, K., Peck, A., Fahad, H.M., Ota, H., Shiraki, H., Kiriya, D., 2016a. Nature 529 (7587), 509–514.
Gao, W., Nyein, H.Y.Y., Shahpar, Z., Fahad, H.M., Chen, K., Emaminejad, S., Gao, Y., Tai, L.-C., Ota, H., Wu, E., Bullock, J., Zeng, Y., Lien, D.-H., Javey, A., 2016b. ACS Sens. 1 (7), 866–874.
Gao, Y., Ota, H., Schaler, E.W., Chen, K., Zhao, A., Gao, W., Fahad, H.M., Leng, Y., Zheng, A., Xiong, F., Zhang, C., Tai, L.C., Zhao, P., Fearing, R.S., Javey, A., 2017. Adv. Mater. 29 (39), 1701985.
Gao, L., Zhang, Y., Malyarchuk, V., Jia, L., Jang, K.I., Webb, R.C., Fu, H., Shi, Y., Zhou, G., Shi, L., Shah, D., Huang, X., Xu, B., Yu, C., Huang, Y., Rogers, J.A., 2014. Nat. Commun. 5, 4938.
Gladman, A.S., Matsumoto, E.A., Nuzzo, R.G., Mahadevan, L., Lewis, J.A., 2016. Nat. Mater. 15 (4), 413–418.
Gonzalez, F., Boue, S., Belmonte, J.C.I., 2011. Nat. Rev. Genet. 12 (4), 231–242.
Han, S., Kim, J., Won, S.M., Ma, Y., Kang, D., Xie, Z., Lee, K.-T., Chung, H.U., Banks, A., Min, S., 2018. Sci. Transl. Med. 10 (435), eaan4950.
Heikenfeld, J., 2016. Electroanalysis 28 (6), 1242–1249.
Heikenfeld, J., Jajack, A., Rogers, J., Gutruf, P., Tian, L., Pan, T., Li, R., Khine, M., Kim, J., Wang, J., 2018. Lab Chip 18 (2), 217–248.
Henry, S., McAllister, D.V., Allen, M.G., Prausnitz, M.R., 1999. J. Pharm. Sci. 88 (9), 948.
Henslee, B.E., Morss, A., Hu, X., Lafyatis, G.P., Lee, L.J., 2011. Anal. Chem. 83 (11), 3998–4003.
Hong, S., Lee, H., Lee, J., Kwon, J., Han, S., Suh, Y.D., Cho, H., Shin, J., Yeo, J., Ko, S.H., 2015. Adv. Mater. 27 (32), 4744–4751.
Huang, D., Zhao, D.Y., Wang, X.X., Li, C.H., Yang, T.R., Du, L.L., Wei, Z.W., Cheng, Q., Cao, H.Q., Liang, Z.C., Huang, Y.Y., Li, Z.H., 2018. Theranostics 8 (9), 2361–2376.
Imani, S., Bandodkar, A.J., Mohan, A.V., Kumar, R., Yu, S., Wang, J., Mercier, P.P., 2016. Nat. Commun. 7, 11650.
Jain, A.K., Lee, C.H., Gill, H.S., 2016. J. Control Release 239, 72–81.
Jang, K.I., Jung, H.N., Lee, J.W., Xu, S., Liu, Y.H., Ma, Y., Jeong, J.W., Song, Y.M., Kim, J., Kim, B.H., Banks, A., Kwak, J.W., Yang, Y., Shi, D., Wei, Z., Feng, X., Paik, U., Huang, Y., Ghaffari, R., Rogers, J.A., 2016. Adv. Funct. Mater. 26 (40), 7281–7290.
Jeong, G.S., Baek, D.-H., Jung, H.C., Song, J.H., Moon, J.H., Hong, S.W., Kim, I.Y., Lee, S.-H., 2012. Nat. Commun. 3, 977.
Jeong, J.W., Kim, M.K., Cheng, H., Yeo, W.H., Huang, X., Liu, Y., Zhang, Y., Huang, Y., Rogers, J.A., 2014. Adv. Healthc. Mater. 3 (5), 642–648.
Jeong, J.W., Yeo, W.H., Akhtar, A., Norton, J.J., Kwack, Y.J., Li, S., Jung, S.Y., Su, Y., Lee, W., Xia, J., 2013. Adv. Mater. 25 (47), 6839–6846.
Kabir, M.M., Perez-Alday, E.A., Thomas, J., Sedaghat, G., Tereshchenko, L.G., 2017. J. Electrocardiol. 50 (3), 342–348.
Kang, S.-K., Murphy, R.K., Hwang, S.-W., Lee, S.M., Harburg, D.V., Krueger, N.A., Shin, J., Gamble, P., Cheng, H., Yu, S., 2016. Nature 530 (7588), 71–76.
Kearney, M.-C., Brown, S., McCrudden, M.T., Brady, A.J., Donnelly, R.F., 2014. Photo. Photodyn. 11 (4), 459–466.
Khan, Y., Ostfeld, A.E., Lochner, C.M., Pierre, A., Arias, A.C., 2016. Adv. Mater. 28 (22), 4373–4395.
Kim, J., Gutruf, P., Chiarelli, A.M., Heo, S.Y., Cho, K., Xie, Z., Banks, A., Han, S., Jang, K.I., Lee, J.W., 2017. Adv. Funct. Mater. 27 (1), 1604373.
Kim, D.-H., Lu, N., Ma, R., Kim, Y.-S., Kim, R.-H., Wang, S., Wu, J., Won, S.M., Tao, H., Islam, A., 2011. Science 333 (6044), 838–843.
Kim, B.J., Meng, E., 2016. J. Micromech. Microeng. 26 (1), 013001.
Kim, Y.C., Park, J.H., Prausnitz, M.R., 2012. Adv. Drug Deliv. Rev. 64 (14), 1547–1568.
King, R., 2004. Methods Mol. Biol. 245, 167–174.
Koh, A., Kang, D., Xue, Y., Lee, S., Pielak, R.M., Kim, J., Hwang, T., Min, S., Banks, A., Bastien, P., 2016. Sci. Transl. Med. 8 (366) (366ra165–366ra165).
Konermann, S., Brigham, M.D., Trevino, A.E., Joung, J., Abudayyeh, O.O., Barcena, C., Hsu, P.D., Habib, N., Gootenberg, J.S., Nishimasu, H., Nureki, O., Zhang, F., 2015. Nature 517 (7536) (583-U332).
Lee, S.M., Byeon, H.J., Lee, J.H., Baek, D.H., Lee, K.H., Hong, J.S., Lee, S.-H., 2014. Sci. Rep. 4, 6074.
Lee, H., Choi, T.K., Lee, Y.B., Cho, H.R., Ghaffari, R., Wang, L., Choi, H.J., Chung, T.D., Lu, N., Hyeon, T., 2016a. Nat. Nanotechnol. 11 (6), 566–572.
Lee, H., Song, C., Baik, S., Kim, D., Hyeon, T., Kim, D.H., 2017. Adv. Drug Deliv. Rev. 127, 35–45.
Lee, J.W., Xu, R., Lee, S., Jang, K.I., Yang, Y., Banks, A., Yu, K.J., Kim, J., Xu, S., Ma, S., Jang, S.W., Won, P., Li, Y., Kim, B.H., Choe, J.Y., Huh, S., Kwon, Y.H., Huang, Y., Paik, U., Rogers, J.A., 2016b. Proc. Natl. Acad. Sci. USA 113 (22), 6131–6136.
Levine, B.L., 2015. Cancer Gene Ther. 22 (2), 79–84.
Lewis, J.A., Ahn, B.Y., 2015. Nature 518 (7537), 42.
Li, J., Zhang, C., Duan, L., Zhang, L.M., Wang, L.D., Dong, G.F., Wang, Z.L., 2016. Adv. Mater. 28 (1), 106–110.
Liang, X., Boppart, S.A., 2010. IEEE Trans. Bio-Med. Eng. 57 (4), 953–959.
Liu, Y., Norton, J.J., Qazi, R., Zou, Z., Ammann, K.R., Liu, H., Yan, L., Tran, P.L., Jang, K.-I., Lee, J.W., 2016. Sci. Adv. 2 (11), e1601185.
Liu, Y., Pharr, M., Salvatore, G.A., 2017. ACS Nano 11 (10), 9614–9635.
Liu, X., Yuk, H., Lin, S., Parada, G.A., Tang, T.C., Tham, E., de la Fuente-Nunez, C., Lu, T.K., Zhao, X., 2018. Adv. Mater. 30 (4), 1704821.
Lochner, C.M., Khan, Y., Pierre, A., Arias, A.C., 2014. Nat. Commun. 5, 5745.
Lu, N., Kim, D.-H., 2014. Soft Robot 1 (1), 53–62.
Lu, L., Yang, Z., Meacham, K., Cvetkovic, C., Corbin, E.A., Vázquez-Guardado, A., Xue, M., Yin, L., Boroumand, J., Pakeltis, G., 2018. Adv. Energy Mater. 8 (16), 1703035.
Luo, N., Dai, W., Li, C., Zhou, Z., Lu, L., Poon, C.C.Y., Chen, S.-C., Zhang, Y., Zhao, N., 2016. Adv. Funct. Mater. 26 (8), 1178–1187.
Martin, A., Kim, J., Kurniawan, J.F., Sempionatto, J.R., Moreto, J.R., Tang, G., Campbell, A.S., Shin, A., Lee, M.Y., Liu, X., Wang, J., 2017. ACS Sens. 2 (12), 1860–1868.
Martín, A., Kim, J., Kurniawan, J.F., Sempionatto, J.R., Moreto, J.R., Tang, G., Campbell, A.S., Shin, A., Lee, M.Y., Liu, X., 2017. ACS Sens. 2 (12), 1860–1868.
Marx, V., 2015. Nat. Methods 12 (1), 41–44.
McAllister, D.V., Wang, P.M., Davis, S.P., Park, J.H., Canatella, P.J., Allen, M.G., Prausnitz, M.R., 2003. Proc. Natl. Acad. Sci. USA 100 (24), 13755–13760.
Mehier-Humbert, S., Guy, R.H., 2005. Adv. Drug Deliv. Rev. 57 (5), 733–753.
Mishra, R.K., Hubble, L.J., Martín, A., Kumar, R., Barfidokht, A., Kim, J., Musameh, M.M., Kyratzis, I.L., Wang, J., 2017. ACS Sens. 2 (4), 553–561.
Mishra, R.K., Martin, A., Nakagawa, T., Barfidokht, A., Lu, X., Sempionatto, J.R., Lyu, K.M., Karajic, A., Musameh, M.M., Kyratzis, I.L., 2018. Biosens. Bioelectron. 101, 227–234.
Mitragotri, S., 2005. Nat. Rev. Drug Discov. 4 (3), 255–260.
Mitragotri, S., Blankschtein, D., Langer, R., 1995. Science 269 (5225), 850–853.
Mitragotri, S., Kost, J., 2004. Adv. Drug Deliv. Rev. 56 (5), 589–601.
Miyamoto, A., Lee, S., Cooray, N.F., Lee, S., Mori, M., Matsuhisa, N., Jin, H., Yoda, L., Yokota, T., Itoh, A., 2017. Nat. Nanotechnol. 12 (9), 907–913.
Moh, J.H., Kim, M.J., Kim, Y.T., Khang, G., Lee, T.W., Lee, H.K., Lee, H.B., 2009. Tissue Eng. Regen. Med. 6 (14) (1447-1447).
Mostafalu, P., Sonkusale, S., 2015. RSC Adv. 5 (12), 8680–8687.
Myers, A.C., Huang, H., Zhu, Y., 2015. RSC Adv. 5 (15), 11627–11632.
Nag, A., Mukhopadhyay, S.C., 2015. Wearable electronics sensors: Current status and future opportunities. In: Wearable Electronics Sensors, Springer, pp. 1–35.
Nejad, S.M., Hosseini, H., Akiyama, H., Tachibana, K., 2016. Theranostics 6 (4), 446–455.
Ota, H., Chen, K., Lin, Y., Kiriya, D., Shiraki, H., Yu, Z., Ha, T.J., Javey, A., 2014. Nat. Commun. 5, 5032.
Pandey, S., Shah, R., Mewada, A., Thakur, M., Oza, G., Sharon, M., 2013. J. Mater. Sci. Mater. Med. 24 (7), 1671–1681.
Pang, C., Lee, C., Suh, K.Y., 2013. J. Appl. Polym. Sci. 130 (3), 1429–1441.
Park, S., Kim, Y.S., Kim, W.B., Jon, S., 2009. Nano Lett. 9 (4), 1325–1329.
Patel, S., Park, H., Bonato, P., Chan, L., Rodgers, M., 2012. J. Neuroeng. Rehabil. 9 (1), 21.
Paudel, K.S., Milewski, M., Swadley, C.L., Brogden, N.K., Ghosh, P., Stinchcomb, A.L., 2010. Ther. Deliv. 1 (1), 109–131.
Paulussen, E.J.M., Zhou, G., Jansen, M.Y., Dekker, T., Beckers, L.J.A.M., Van Pieterson, L., Van Pieterson, L., 2015. Wearable and breathable photo therapy patch. Google Patents.
Pires, M.T.F., Nogueira, L.R., Issa, M.C.A., 2018. Lasers Lights Other Technol. 473.
Prausnitz, M.R., 2004. Adv. Drug Deliv. Rev. 56 (5), 581–587.
Prausnitz, M.R., 2017. Annu. Rev. Chem. Biomol. Eng. 8, 177–200.
Prausnitz, M.R., Langer, R., 2008. Nat. Biotechnol. 26 (11), 1261–1268.
Prausnitz, M.R., Mitragotri, S., Langer, R., 2004. Nat. Rev. Drug Discov. 3 (2), 115–124.
Rogers, J., Lagally, M., Nuzzo, R., 2011. Nature 477 (7362), 45–53.
Rogers, J.A., Nuzzo, R.G., 2005. Mater. Today 8 (2), 50–56.
Rogers, J.A., Someya, T., Huang, Y., 2010. Science 327 (5973), 1603–1607.
Salvo, P., Di Francesco, F., Costanzo, D., Ferrari, C., Trivella, M.G., De Rossi, D., 2010. IEEE Sens. J. 10 (10), 1557–1558.
Sanjay, S.T., Zhou, W., Dou, M.W., Tavakoli, H., Ma, L., Xu, F., Li, X.J., 2018. Adv. Drug Deliv. Rev. 128, 3–28.
Selvaraj, N., 2015. Proceedings of the 37th Annual International Conference of the IEEE, pp. 3137–3140.
Shalem, O., Sanjana, N.E., Hartenian, E., Shi, X., Scott, D.A., Mikkelsen, T.S., Heckl, D., Ebert, B.L., Root, D.E., Doench, J.G., Zhang, F., 2014. Science 343 (6166), 84–87.
Shim, A., Rogers, J., Hua, F., 2014. Soft lithographic molding of surface relief output couplers for organic light emitting diodes. Google Patents.
Son, D., Lee, J., Qiao, S., Ghaffari, R., Kim, J., Lee, J.E., Song, C., Kim, S.J., Lee, D.J., Jun, S.W., 2014. Nat. Nanotechnol. 9 (5), 397–404.
Stolik, S., Delgado, J., Perez, A., Anasagasti, L., 2000. J. Photochem. Photobiol. B 57 90–93 (2–3).
Stoppa, M., Chiolerio, A., 2014. Sensors 14 (7), 11957–11992.
Sullivan, S.P., Koutsonanos, D.G., Martin, M.D., Lee, J.W., Zarnitsyn, V., Choi, S.O., Murthy, N., Compans, R.W., Skountzou, I., Prausnitz, M.R., 2010. Nat. Med. 16 (8) (915-U116).
Sun, Y., Choi, W.M., Jiang, H., Huang, Y.Y., Rogers, J.A., 2006. Nat. Nanotechnol. 1 (3), 201–207.
Tee, B.C.-K., Chortos, A., Berndt, A., Nguyen, A.K., Tom, A., McGuire, A., Lin, Z.C., Tien, K., Bae, W.-G., Wang, H., 2015. Science 350 (6258), 313–316.
Tian, L., Li, Y., Webb, R.C., Krishnan, S., Bian, Z., Song, J., Ning, X., Crawford, K., Kurniawan, J., Bonifas, A., Ma, J., Liu, Y., Xie, X., Chen, J., Liu, Y., Shi, Z., Wu, T., Ning, R., Li, D., Sinha, S., Cahill, D.G., Huang, Y., Rogers, J.A., 2017. Adv. Funct. Mater. 27 (26), 1701282.
Trung, T.Q., Lee, N.E., 2016. Adv. Mater. 28 (22), 4338–4372.
Trung, T.Q., Ramasundaram, S., Hwang, B.U., Lee, N.E., 2016. Adv. Mater. 28 (3), 502–509.
Valentine, A.D., Busbee, T.A., Boley, J.W., Raney, J.R., Chortos, A., Kotikian, A., Berrigan, J.D., Durstock, M.F., Lewis, J.A., 2017. Adv. Mater. 29 (40), 1703817.
VanDersarl, J.J., Xu, A.M., Melosh, N.A., 2012. Nano Lett. 12 (8), 3881–3886.
Vecchione, R., Coppola, S., Esposito, E., Casale, C., Vespini, V., Grilli, S., Ferraro, P., Netti, P.A., 2014. Adv. Funct. Mater. 24 (23), 3515–3523.
Wang, H.-P., Guo, A.-W., Bi, Z.-Y., Li, F., Lü, X.-Y., Wang, Z.-G., 2017a. Proceedings of the 39th Annual International Conference of the IEEE, pp. 714–717.
Wang, H.-P., Guo, A.-W., Zhou, Y.-X., Xia, Y., Huang, J., Xu, C.-Y., Huang, Z.-H., Lü, X.-Y.,

Wang, Z.-G., 2017b. Int. J. Electron. 104 (9), 1514–1526.
Wang, M., Hu, L., Xu, C., 2017d. Lab Chip 17 (8), 1373–1387.
Wang, L., Jackman, J.A., Park, J.H., Tan, E.-L., Cho, N.-J., 2017c. J. Mater. Chem. B 5 (22), 4019–4024.
Wang, H., Pastorin, G., Lee, C., 2016a. Adv. Sci. 3 (9), 1500441.
Wang, S.W., Zhao, X.Y., Wang, S.C., Qian, J., He, S.L., 2016b. ACS Appl. Mater. Interfaces 8 (37), 24368–24384.
Wang, Y., Zhu, C., Pfattner, R., Yan, H., Jin, L., Chen, S., Molina-Lopez, F., Lissel, F., Liu, J., Rabiah, N.I., 2017e. Sci. Adv. 3 (3), e1602076.
Webb, R.C., Bonifas, A.P., Behnaz, A., Zhang, Y., Yu, K.J., Cheng, H., Shi, M., Bian, Z., Liu, Z., Kim, Y.S., Yeo, W.H., Park, J.S., Song, J., Li, Y., Huang, Y., Gorbach, A.M., Rogers, J.A., 2013. Nat. Mater. 12 (10), 938–944.
Webb, R.C., Pielak, R.M., Bastien, P., Ayers, J., Niittynen, J., Kurniawan, J., Manco, M., Lin, A., Cho, N.H., Malyrchuk, V., Balooch, G., Rogers, J.A., 2015. PLoS One 10 (2), e0118131.
Wei, Z.W., Zheng, S.Q., Wang, R.X., Bu, X.L., Ma, H.L., Wu, Y.D., Zhu, L., Hu, Z.Y., Liang, Z.C., Li, Z.H., 2014. Lab Chip 14 (20), 4093–4102.
Windmiller, J.R., Wang, J., 2013. Electroanalysis 25 (1), 29–46.
Wu, X., Ma, Y., Zhang, G., Chu, Y., Du, J., Zhang, Y., Li, Z., Duan, Y., Fan, Z., Huang, J., 2015a. Adv. Funct. Mater. 25 (14), 2138–2146.
Wu, Y.C., Wu, T.H., Clemens, D.L., Lee, B.Y., Wen, X.M., Horwitz, M.A., Teitell, M.A., Chiou, P.Y., 2015b. Nat. Methods 12 (5), 439–444.
Xia, Y., Whitesides, G.M., 1998. Annu Rev. Mater. Sci. 28 (1), 153–184.
Xie, C., Lin, Z., Hanson, L., Cui, Y., Cui, B., 2012. Nat. Nanotechnol. 7 (3), 185–190.
Xu, X., Akay, A., Wei, H., Wang, S., Pingguan-Murphy, B., Erlandsson, B.-E., Li, X., Lee, W., Hu, J., Wang, L., 2015. Proceedings of the IEEE, vol. 103(2), pp. 236–247.
Xu, B., Akhtar, A., Liu, Y., Chen, H., Yeo, W.H., Park, S.I., Boyce, B., Kim, H., Yu, J., Lai, H.Y., 2016. Adv. Mater. 28 (22), 4462–4471.
Xu, S., Zhang, Y., Jia, L., Mathewson, K.E., Jang, K.-I., Kim, J., Fu, H., Huang, X., Chava, P., Wang, R., 2014. Science 344 (6179), 70–74.
Yamada, T., Hayamizu, Y., Yamamoto, Y., Yomogida, Y., Izadi-Najafabadi, A., Futaba, D.N., Hata, K., 2011. Nat. Nanotechnol. 6 (5), 296–301.
Yamamoto, Y., Yamamoto, D., Takada, M., Naito, H., Arie, T., Akita, S., Takei, K., 2017. Adv. Healthc. Mater. 6 (17), 1700495.
Yan, L., Yang, Y., Zhang, W., Chen, X., 2014. Adv. Mater. 26 (31), 5533–5540.
Yang, S., Chen, Y.C., Nicolini, L., Pasupathy, P., Sacks, J., Su, B., Yang, R., Sanchez, D., Chang, Y.F., Wang, P., 2015. Adv. Mater. 27 (41), 6423–6430.
Yang, T., Xie, D., Li, Z., Zhu, H., 2017. Mater. Sci. Eng. R 115, 1–37.
Yeo, J., Kim, G., Hong, S., Kim, M.S., Kim, D., Lee, J., Lee, H.B., Kwon, J., Suh, Y.D., Kang, H.W., 2014. J. Power Sources 246, 562–568.
Yeo, W.H., Kim, Y.S., Lee, J., Ameen, A., Shi, L., Li, M., Wang, S., Ma, R., Jin, S.H., Kang, Z., 2013. Adv. Mater. 25 (20), 2773–2778.
Yokota, T., Inoue, Y., Terakawa, Y., Reeder, J., Kaltenbrunner, M., Ware, T., Yang, K., Mabuchi, K., Murakawa, T., Sekino, M., 2015. Proc. Natl. Acad. Sci. USA 112 (47), 14533–14538.
Yokota, T., Zalar, P., Kaltenbrunner, M., Jinno, H., Matsuhisa, N., Kitanosako, H., Tachibana, Y., Yukita, W., Koizumi, M., Someya, T., 2016. Sci. Adv. 2 (4), e1501856.
Yu, Y., Zhang, J., Liu, J., 2013. PLoS One 8 (3), e58771.
Yuana, Y., Jiang, L.L., Lammertink, B.H.A., Vader, P., Deckers, R., Bos, C., Schiffelers, R.M., Moonen, C.T., 2017. Int. J. Mol. Sci. 18 (8), E1610.
Zhang, Z.X., Wang, Y.Y., Zhang, H.X., Tang, Z.F., Liu, W.P., Lu, Y., Wang, Z.F., Yang, H.T., Pang, W., Zhang, H., Zhang, D.H., Duan, X.X., 2017b. Small 13 (18), 1602962.
Zhang, F., Zang, Y., Huang, D., Di, C.A., Zhu, D., 2015. Nat. Commun. 6, 8356.
Zhang, Y., Zhang, F., Yan, Z., Ma, Q., Li, X., Huang, Y., Rogers, J.A., 2017a. Nat. Rev. Mater. 2 (4), 17019.
Zhao, Y., Huang, X., 2017. Micromachines 8 (3), 69.
Zhu, X.Y., Kwok, S.Y., Yuen, M.F., Yan, L., Chen, W., Yang, Y., Wang, Z.G., Yu, K.N., Zhu, G.Y., Zhang, W.J., Chen, X.F., 2015. J. Mater. Sci. 50 (23), 7800–7807.
Zhu, Z., Li, R., Pan, T., 2018. Adv. Mater. 30 (6), 1705122.